TITLE

Bone Marrow Lesions and Subchondral Cysts in Association with Severity of Structural Degeneration in Hip Osteoarthritis

A thesis submitted in partial fulfilment of the degree of BACHELOR OF HEALTH AND MEDICAL SCIENCES (HONOURS)

in the Discipline of Orthopaedics and Trauma, Adelaide Medical School

Faculty of Health Sciences

The University of Adelaide

by

Bright Nkrumah

June 2020

Word count: 4400

SUMMARY

Objective: This study aimed to explore the structural aspects of bone quality in bone marrow lesions (BMLs) and subchondral cysts and to determine the association with structural progression in hip osteoarthritis (OA).

Design: Six femoral heads from patients with OA at total hip arthroplasty and seven age-matched NoOA cadaveric controls, were scanned *ex vivo* by MRI to identify BMLs and cysts and evaluate cartilage volume, micro-CT imaged to quantitate the subchondral (plate and trabecular) bone microstructure in four regions (anterior superior [AS], anterior inferior [AI], posterior superior [PS] and posterior inferior [PI]) and imaged by synchrotron micro-CT to further assess bone vasculature and osteocyte lacunar.

Results: BMLs and cysts in the OA femoral head were predominantly located in the anterior regions ([AS] and [AI]). Overall intragroup differences in microstructure were not significant. In the OA group, AS and AI regions, followed by (PS) region contained the most structural alterations. Comparing OA to NoOA, we found that AS region of the OA group had significantly thicker subchondral bone plate ($P < .0001$, $P < .05$), thicker trabeculae ($P < .0001$, $P < .05$), and denser vascular canals ($P < .05$).

Conclusion: In advanced hip OA microstructural deterioration of the subchondral bone was in association with the presence of BMLs and cysts. Therefore, the use of BMLs and subchondral bone cysts as MRI image-based biomarkers may provide information on the progressive state of OA within the cartilage-subchondral bone unit.

INTRODUCTION

Osteoarthritis (OA) is a common musculoskeletal joint disease, predominantly affecting the knee, hand and hip, which results in pain and often renders mobility problems in individuals aged 50 and above [1-4]. Primary OA is the degeneration of an intact articular joint with no external influence while secondary OA is caused by certain factors such as obesity, genes and trauma, to mention a few. Symptoms of OA include general joint pain and groin pain specific to hip OA[3, 5].

Current treatments are limited to pain management drugs such as paracetamol and nonsteroidal anti-inflammatory drugs (NSAIDs) in conjunction with lifestyle changes such as weight reduction and aquatic exercising with joint replacement surgery (arthroplasty) in late stages of the disease[5-7]. Excitingly, the research has shifted to the development of disease-modifying drugs, which can modify structural changes (subchondral bone remodelling and regrowing lost cartilage) in both the subchondral bone and cartilage respectively[7].

Pathogenesis of Osteoarthritis

There are two opposing ideas about the pathogenesis of OA in the literature. One is the cartilage-driven OA, and the second is cartilage-subchondral bone (osteochondral) driven. For the cartilage-driven OA, studies have proposed injury to cartilage results in chondrocyte cluster formation, increased pro-inflammatory factor release and proteoglycan and collagen network depletion as the disease progresses to late stage[5, 8]. In the osteochondral driven studies, there have been suggestions that cartilage matrix alteration and subchondral bone remodelling in response to biomechanical loading occurs at the same time[9]. The bone changes include subchondral bone plate thinning at the early stage of the disease[4, 10] and subsequent plate and trabecular bone thickening (sclerosis) in late or advanced stage[4, 11]. Additionally, the increased porosity, bone formation at the margins (osteophyte), subchondral cysts and bone marrow lesions formation, which appear to be sclerotic in comparison to unaffected areas are as a result of the increased trabecular thickness and bone volume fraction[12]. Concurrently, micro-damage in the form of micro-cracks occurring through the non-calcified cartilage, tidemark, calcified cartilage and the subchondral bone plate results in the growth of vascular tissues and nerve cells from the subchondral

bone up via the micro-cracks into the articular cartilage[5, 8]. This suggests that there is an exchange of biochemical molecules between the bone and cartilage[5, 8, 13, 14]. However, hip subchondral bone microstructure (inclusive of bone microarchitecture, vascularity and microdamage), bone mineralisation as well as the molecules involved in the crosstalk is not entirely known[8].

Subchondral cyst and bone marrow lesion

Over the years X-ray has been used predominantly (in the knee) as the primary clinical diagnostic tool for assessment of OA parameters such as joint space narrowing and subchondral cyst, but its lower 2-dimensional resolution and irradiation has been its limitation[15, 16]. Later emergence of MRI as a diagnostic tool provided a better opportunity to establish an association between OA severity and progression and the disease parameters such as osteophyte formation, cartilage defects and loss as well as subchondral BMLs and cysts formation in the knee and hip OA[17-20]. However, despite its advantages, it is also limited by low resolution. Micro-CT is another imaging technique that has been used to evaluate subchondral bone density, osteophyte and subchondral cyst formation in both knee and hip OA. Despite micro-CT's ability to analyse trabecular bone architecture in different 3-dimensional planes, it is also limited by higher irradiation[13].

Subchondral cysts defined as a zone of well-demarcated hyper signal located in the subchondral bone adjacent intimately to the articular cartilage and visible on the fluid-sensitive MR sequence and T1 low field MR sequence[21]. Many studies have suggested that cyst formation occurs through either fluid intrusion or bone resorption /contusion theory, which have been well described in the literature[22-24]. Cysts have been suggested to be associated with low bone mineralisation[25] and shown to occur more often in the late stage of OA[26]. Subchondral cysts have also been found to be correlated with BMLs in the late stages of hip OA.

BMLs are defined as irregular areas of increased signal intensity on the fluid-sensitive MR sequence and decreased intensity on T1 low field MR sequence[27, 28]. They characterised by oedema, fibrosis and necrosis at histopathology and contributed to the loss of articular cartilage and hip OA progression[27, 28]. Cross-sectional studies using MRI imaging techniques have found an association between cartilage

defects and loss, and BMLs in both individuals with and without hip OA at the anterior and superior regions of the femoral head[29]. In the same study, the authors suggested that the more significant cartilage defect and the subsequent volume loss was found in individuals with hip OA compared to those without cartilage defects[29]. This finding suggested that MRI detected cartilage defects and BMLs might have occurred before individuals presenting with clinical OA symptoms such as pain. Longitudinal studies have reported MRI images of hip OA to be correlated with histopathological BMLs and cysts assessment. It has been suggested that increased subchondral cyst size and number was significantly higher amongst OA patients. Moreover, increase BML, and subchondral cyst size is associated with worsening of hip pain [21, 28, 30-34]. Taken together, clinical studies have provided invaluable information on the association of the cysts and BMLs with OA. However, the nature of these pathologies at tissue level is poorly understood[35].

In this study, we used advanced imaging modalities, micro-CT to quantify trabecular bone microarchitecture and synchrotron radiation micro-CT, a novel imaging technique with a higher spatial resolution while maintaining excellent signal to noise ratio and a higher power quantitative capability (in 3D)[36, 37], to investigate bone quality *ex vivo* in femoral head subchondral bone areas where BMLs and cysts are found in hip OA. This technique will enable the visualisation of vascular canals and osteocyte lacunar, which have been suggested to interact with each other through dendritic processes and play a significant role in OA progression[38, 39]. We hypothesised that subchondral bone pathologies, BMLs and cysts, are indicative of different tissue processes and directly associated with different severity of structural degeneration within osteochondral tissue for hip OA. Thus, this study aimed to explore the structural aspect of bone quality in BMLs and subchondral cysts and determine the association with structural progression in hip OA.

MATERIALS AND METHODS

Study participants: Hip OA patients and Cadavers

This project involved the use of 6 femoral heads from patients who had undergone total hip OA joint replacement surgery (South Australia (SA) Tissue Bank, Royal Adelaide Hospital). The control group comprised 7 cadaveric femoral heads obtained through the SA Tissue Bank, SA Pathology-Royal Adelaide Hospital Mortuary, with no previous history of bone or joint disease (Paget's disease, malignant tumours, avascular necrosis, rheumatoid arthritis), or medication that may have affected bone metabolism.

Both experimental and control groups of specimens comprised of an equal number of females and males aged >50 years. Inclusion criteria for the OA group were; individuals with confirmed radiographic OA with severe symptomatic disabilities. Exclusion criteria were individuals with OA due to trauma or rheumatoid arthritis, osteoporosis, as well as metabolic bone diseases.

Written consent was obtained for all participants, and initial approval for the study was received from the Human Research Ethics Committee at the Royal Adelaide Hospital and The University of Adelaide, South Australia, under the Declaration of Helsinki 1975

Imaging techniques

Magnetic Resonance Imaging (MRI) assessment

To detect subchondral bone pathologies (BMLs and subchondral cysts), each femoral head was imaged using MRI *ex vivo* in an 8-channel wrist coil (3T MRI Siemens TRIO, Royal Adelaide Hospital, Adelaide) where two clinically relevant sequences were used. These include fat-suppressed fast spin-echo proton density-weighted (PDFS), and T1 –weighted[40, 41].

A BML as seen in (Fig 1) was defined as a zone of altered signal intensity seen on PDFS, and T1 weighted sequences in the bone marrow, located immediately beneath the articular cartilage and visible on at least two consecutive slices[40-43].

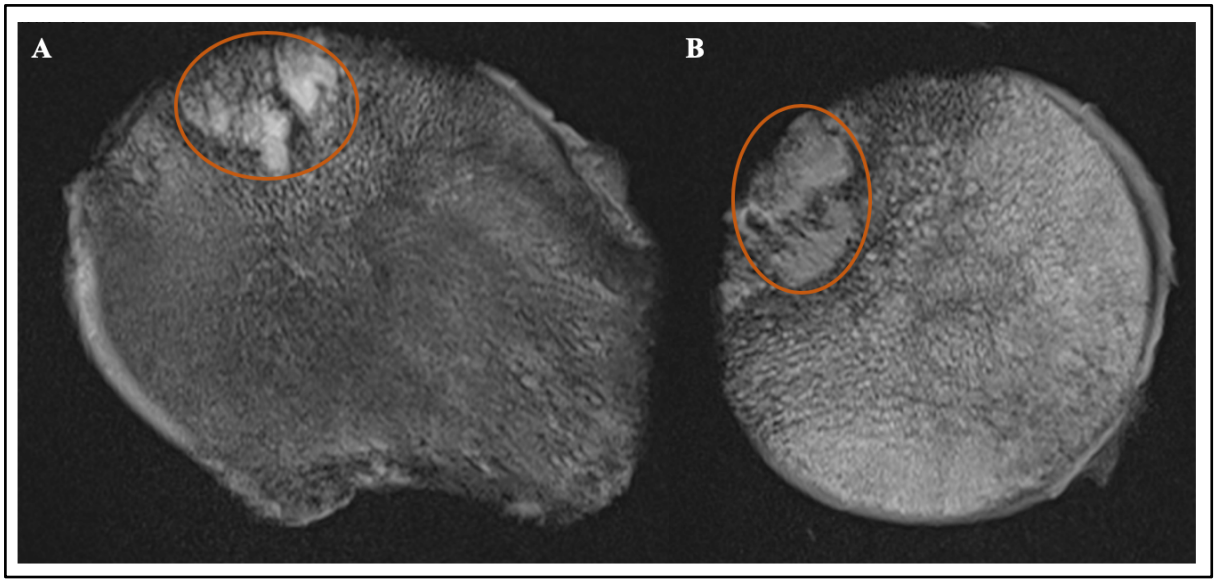

Fig 1. MRI of the femoral head (PDFS/T1 weighted view) of a 69-year-old male hip OA patient taken *ex-vivo* (post hip replacement surgery). BML (within orange oval shape) is visualised as an ill-defined area of hyper-intense signal in PDFS-weighted sequences (A). In T1-weighted sequences the BML appears as a hypo-intense signal (B).

A subchondral cyst (Fig 2) was defined as a well-demarcated hyper-signal.

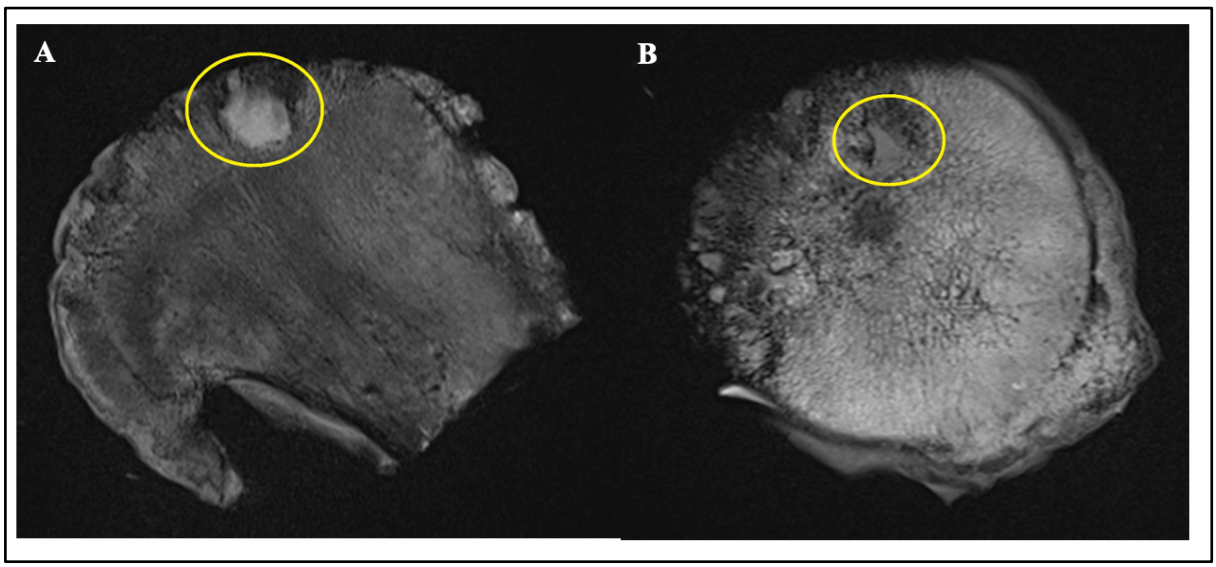

Fig 2. MRI of the femoral head (PDFS/T1-weighted view) of a 48-year-old male hip OA patient taken *ex vivo* (post hip replacement surgery). In PDFS-weighted sequences, a cyst (within yellow oval shape) appears as a well-demarcated hyper-signal. In T1-weighted sequences, cysts are visualised as a well-demarcated hypo-signal.

Three-dimensional (3D) sequences were used to map the frequency and location of bone cysts and BMLs. Cartilage volume was obtained from MRI images[40].

MR images were used to obtain cartilage volume data. Cartilage volume was assessed using the MRI reading software HOROS (Purview, Annapolis, MD USA), and the external contour around the cartilage boundaries of the femoral head was manually marked on the PDFS coronal images, additionally then the automatic volume rendering function was used to calculate the volume in cm^3 (Fig 3). Cyst and BML volume were assessed using Materialised Mimics Research software (Materialise NV, Belgium), and the area defined as cyst and BML was masked manually on the PDFS coronal images (Fig 4). Automatic volume rendering function was used to calculate the volume in mm^3.

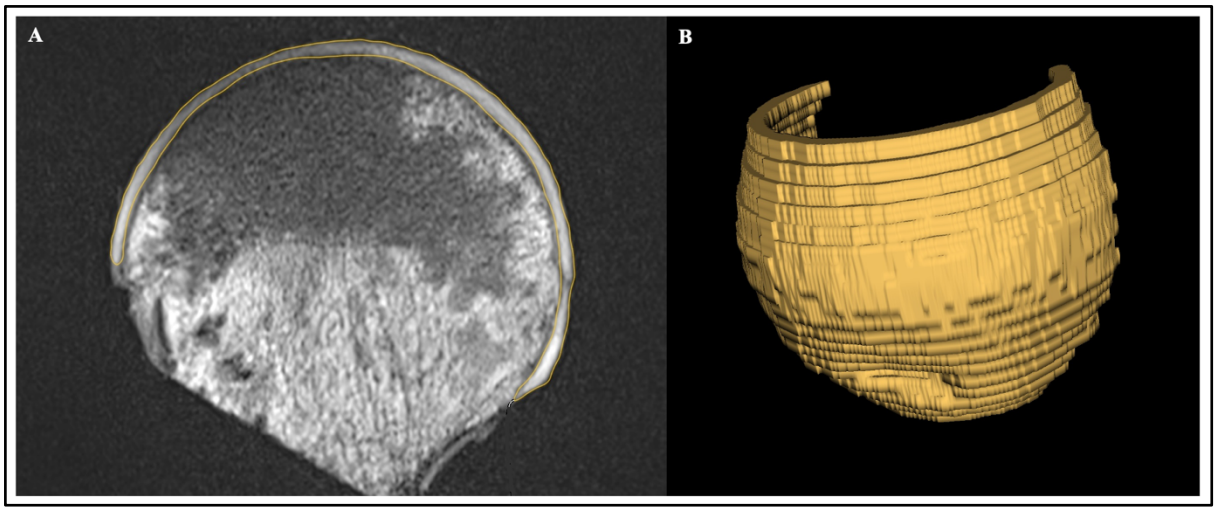

Fig 3. MRI of the femoral head (A-coronal view) of a 50-year-old female hip OA patient taken (post hip replacement surgery). (A) yellow external contour around the cartilage boundaries of the femoral head. (B) 3D image generated via automatic volume rendering of the cartilage.

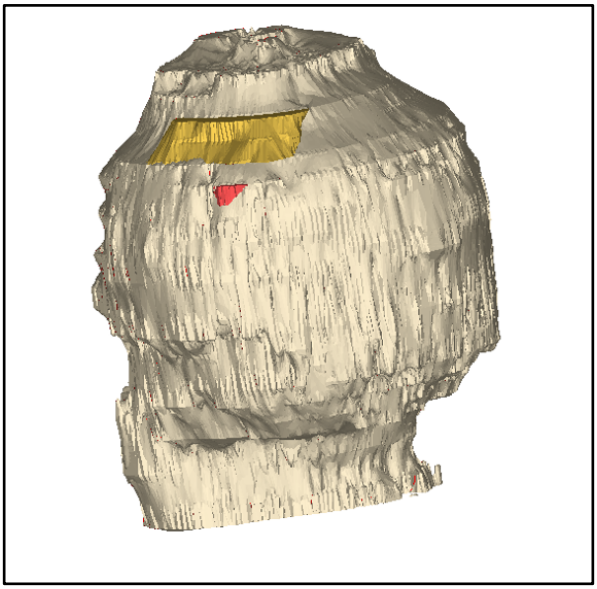

Fig 4. MRI 3D model of femoral head with BML (yellow) and cyst (red).

Miro-computed tomography (micro-CT) imaging

To analyse the microstructure of the subchondral bone in the whole femoral head, each specimen was scanned at a high spatial resolution by micro-CT (Skyscan 1276; Skyscan-Brucker Belgium) at Adelaide Microscopy, The University of Adelaide. Scanner settings were:20.5 μm isotropic pixel size, source voltage 100kVp, current 200μA, rotation step 0.8˚, 180˚ rotation, exposure time 700 ms, 3 frames averaging. An aluminium-copper filter 1.0mm thick was used for beam hardening artefact reduction. Each scan was performed in four consecutive automated steps, imaging one-fourth of the specimen. For each femoral head, this produced a total of 3305 X-ray projection images (826 projection per step), each image 3872 × 3872 pixels in size, saved in 16-bit Tiff format, generating a projection dataset of 24.3 GB, scan duration~ 4 h. The cross images were then reconstructed using a filtered back-projection algorithm (NRecon software, v2.0.4.2, Skyscan-Bruker). The reconstructed images were binarized using adaptive thresholding. The adaptive threshold value was the average of threshold values determined from the histograms of a subset of six representatives (three from each group) specimens and then applied consistently to all the specimens[41].

Micro-CT Image processing

Femoral head images were manually realigned using Data viewer to match its anatomical representation (left and right) in humans. Realigned images were opened in CTAn analyser software (v.1.18.8.0+ 64 bits) to determine the region of interest. A 4 cylindric region of interest (ROI, size 10×10mm) was selected from anterior superior (AS), anterior inferior (AI), posterior superior (PS) and posterior inferior (PI) aspect of the femoral head (Fig 5) and saved as a volume of interest (VOI). For each region of interest, the plate was split from trabecular bone and was evaluated. Plate thickness was manually evaluated, while the remaining parameters were performed separately.

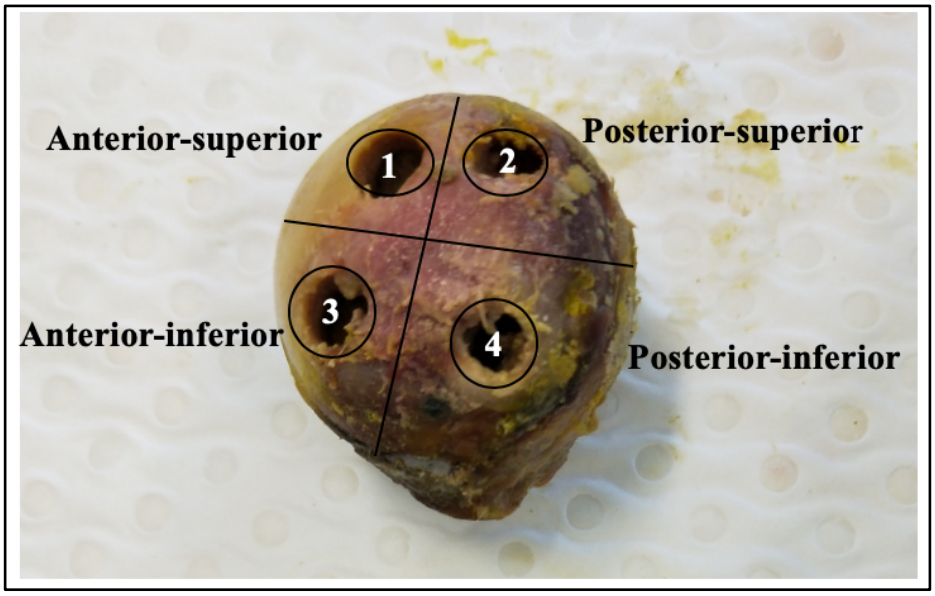

Fig 5. Location of bone cores. The OA bone cores were sampled in areas with and without cartilage according to anatomical locations AS, AI, PS and PI.

Micro-CT morphometric evaluation

Subchondral plate microstructure parameters determined included plate thickness (Pl.Th), porosity (Pl.Po) and percent bone volume (BV/TV), while subchondral trabeculae parameters included: trabecular bone volume (BV/TV,%), which was calculated as the voxels segmented as a bone within VOI, divided by the total number of voxels; trabecular number (Tb.N 1/mm), describing trabeculae per unit length; trabecular thickness (Tb.Th, mm), describing the average 3D thickness of the trabeculae, trabecular separation (Tb.Sp, mm), describing a 3D measure of the mean distance between the

trabeculae, structural model index (SMI), describing the measure of predominant shapes in the plate-like/rod-like structure; trabecular bone pattern factor (Tb.Pf), describing a quantitative ratio of inter-trabecular connectivity; and degree of anisotropy (DA) that depicts the orientation of bone microarchitecture.

Synchrotron radiation computed tomography (Synchrotron micro-CT) imaging

Synchrotron tomographic X-ray experiments were carried out at the X02DA TOMCAT beamline of the Swiss Light Source (SLS) facility at Paul Scherrer Institute (PSI) Switzerland. A monochromatic beam with energy 21keV was used to acquire tomography scans. The X-ray imaging system consisted of a microscope (Optique Peter) with 4× magnification objective and LuAG:CE µm scintillator coupled to a pco.edge 5.5 detector with a pixel size of 1.63µm and filed of view 4.2×3.5 mm^2. For each sample, 1800 projections uniformly distributed over 180 degrees were taken with 120ms exposure each. Tomographic reconstructions were performed on the TOMCAT cluster[44] using phase retrieval method from a single defaced image[45] and GridRec algorithm [46]. Final reconstructed images were saved as 16-bit tiff image stacks. Through the synchrotron radiation X-ray for micro-CT, beam hardening artefact and noise was almost eliminated, and high-quality quantitative assessment of the bone quality of the areas in proximity was obtained. Moreover, the 3D organisation of the vascular canal network and osteocyte lacunae was visualised, counted and measured using CTAn.

Synchrotron micro-CT image processing

We used CTAn analyser software for image processing. An (Otsu) thresholding in 3D space with a radius of 3 methods was applied to the reconstructed trabecular bone to segment the mineralised tissue and non-mineralized structures[47]. Noise (small objects) which did not belong to the bone after thresholding was removed by running sweep function in 3D, removing objects less than 1000 pixels. Afterwards, both blood vessels (open pores) and osteocyte lacunae (closed pores) were closed in the trabecular bone. Thus, it allowed the creation of the region of interest (ROI). A few large pores with an area less than 1800 pixels that remained in the trabecular selection were removed using a 2D despeckled filter in CTAn. Hence, this created ROI for trabecular bone. Subsequently, porosity analysis was

performed using the 3D analysis plugin in custom processing. Closed pores/objects volume ranging from 30-2000µm^3 were considered as osteocyte lacunae (Fig 6.A), and open pores/object volume >2000µm^3 were characterised as vascular canals (Fig 6.B), based on previous studies[47].

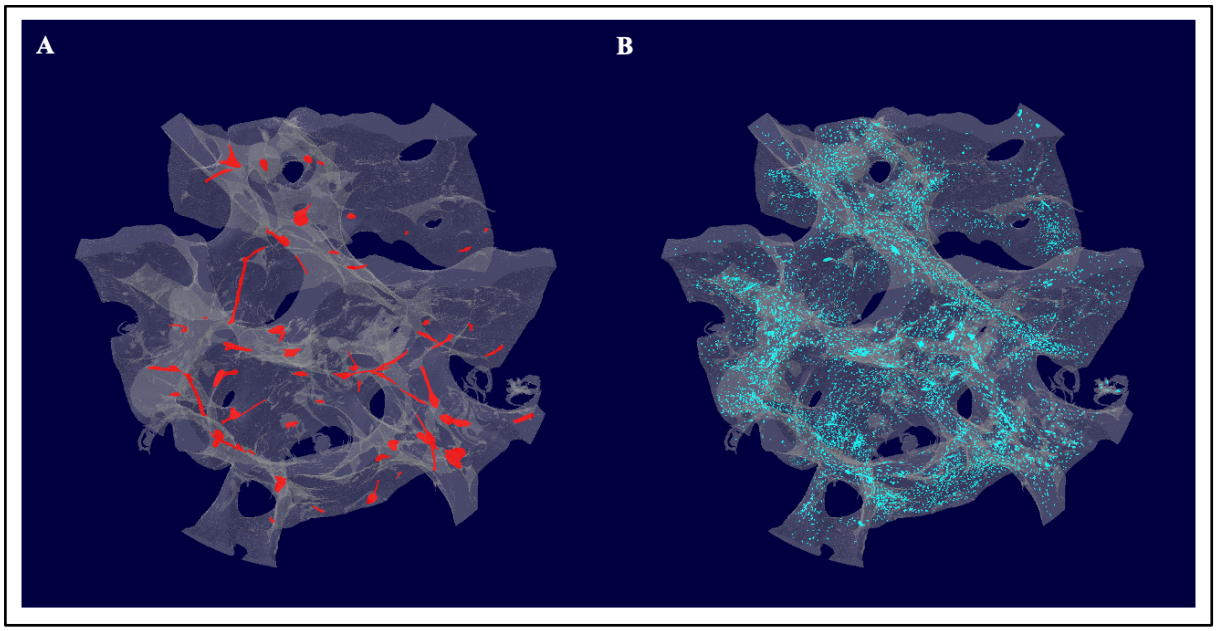

Fig 6. A-B showing 3D models of vascular canals and osteocyte lacunae respectively.

Synchrotron micro-CT 3D morphometric evaluation

Vascular canal parameters quantitatively measured included: Average canal number (ACa.N), canal density (Ca.Dn) which was calculated as Ca.N/BV, canal volume (Ca.V), the ratio of canal volume which was calculated as Ca.V/BV, canal surface (Ca.S), the ratio of canal surface which was calculated as Ca.S/BV and vascular canal diameter.

Osteocyte lacunar parameters were grouped into general, morphological and shape descriptive. Lacunar density (N.Lc/BV) calculated as the number of lacunae over bone volume. Morphological parameters consisted of osteocyte volume and osteocyte surface. Shape descriptive parameters were sphericity (Sph), which is the ratio of the smallest to largest radii and is a measure of lacunar stretch. For complex, non-spherical objects the surface area of the volume-equivalent sphere will be much smaller than the particle surface area; hence Sph will be lower. Sph maximum possible value is 1, which would be obtained for a sphere. Sauter diameter is the diameter of the sphere that would have the same volume-

to-surface (V/S) ratio as a discreet 3D object. Lacunar orientation theta and phi denote the orientation lacunar based on specific angles. For angles between 0-22.5, 22.5-67.5 and 67.5-90, theta and phi will be transverse radial, transverse oblique/ oblique, longitudinal radial/ circumferential respectively.

Synchrotron micro-CT images of each sample were reconstructed into 3D computer models (Fig 7) using image processing software (CTAn plus CTVox v.2.3.2.0. 64 bits).

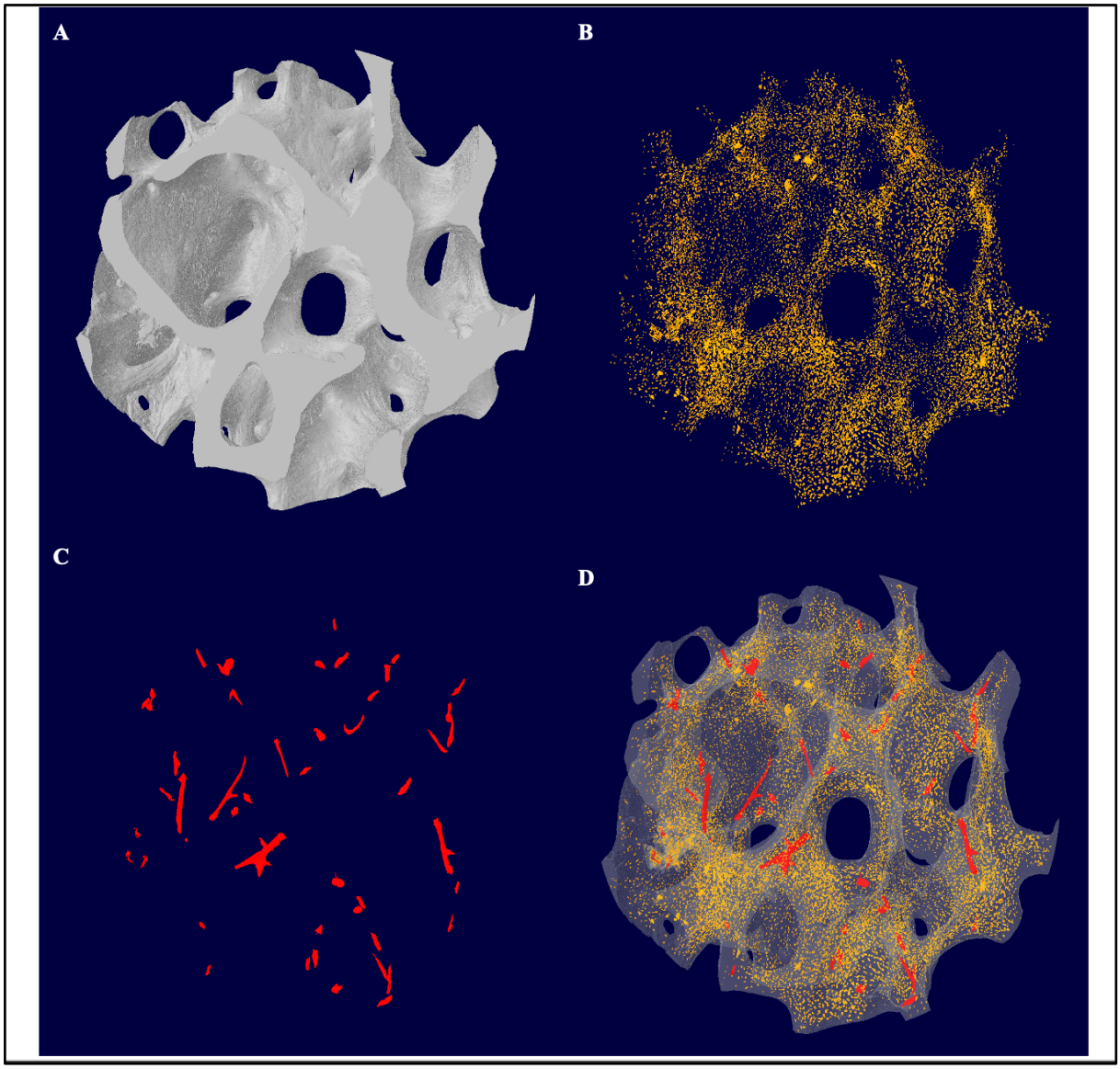

Fig 7. Typical 3D images of A- trabecular bone, B- osteocyte lacunae, C-vascular canals and D-combination of the three components obtained with synchrotron imaging

Statistical Analysis

All data sets were analysed by the Shapiro-Wilk test to determine the normality of the data distribution.

For between-group (NoOA vs OA) comparisons, where variables were continuous normally distributed, an unpaired, two-tailed Student's t-test was used while for continuous non-normally distributed variables; an unpaired, two-tailed Mann-Whitney test was used. Two-way ANOVA (mixed model) with the Turkey test was used for multiple comparisons.

The critical value for statistical significance was chosen as $P<0.05$. These analyses were performed using the GraphPad Prism software (v. 8.4.2, Inc., USA).

RESULTS

Population characteristics

Demographic characteristics and MRI data of participating individuals are summarised in **Table 1**.

MRI Assessment

MRI assessment showed that amongst the 7 subjects in OA-group, 6 (85.71%) contained pathologies (BMLs & cysts) detected by PDFS and T1-weighted sequences in the anterior regions of the femoral head while 1 (14.28%) had no MRI pathology and was excluded. In the NoOA group, 7 (87.50%) had no pathologies, while 1 (12.50%) was excluded based on finding malignant-like pathological changes identified by MRI. The OA-group cartilage volume ranged from 2-5mm^3 with an average of 3.86mm^3, whereas the NoOA group cartilage volume ranged from 3-6mm^3 with an average of 5.08mm^3. Cyst number ranged from 2-12 with an average of 5.3, and Cyst volume ranged from 11-558mm^3 with an average of 270.80mm^3. BML number ranged from 3-13 with an average of 7 and BML volume ranged from 4324-6532mm^3 with an average volume of 2040mm^3.

Table 1

Patients' demographic and MRI data.

	NoOA (n= 7)	OA (n= 6)	*P* value
Age (years)	50.33 ± 5.51	64.43 ± 12.74	.11
Male (%)	3(42.86)	3(50)	NA
Female (%)	4(57.14)	3(50)	NA
Cartilage volume (mm^3)	5.08±0.77	3.86 ± 1.17	.05
Cyst Number	0	5.33 ± 4.46	NA
Cyst Volume (mm^3)	NA	222.6(51.39-533.9)	NA
BML Number	0	7.00 ± 3.65	NA
BML Volume (mm^3)	NA	801.2(432.4-4080)	NA

Mean ± SD; Median (25,75% quartiles

Micro-CT Assessment

Out of the 6 OA group, 1 was excluded due to unknown pathology, and the remaining 5 were assessed. Similarly, the NoOA group were assessed for structural changes or reduction in bone quality. In the OA group, femoral head areas containing BMLs and cyst were compared to corresponding anatomically matched areas in NoOA femoral heads without BMLs and cysts.

Values for percent bone volume and that of plate porosity in PI were excluded due to large osteophyte merging with the plate. Likewise, values for plate thickness in AI, PS and PI regions were excluded. Hence the further reduction in number for those regions.

The results of the subchondral bone plate are illustrated in Fig 8 and 9. There was no significant intragroup variability in mean plate thickness, plate porosity and plate percent bone volume within NoOA and OA groups (Fig.8). However, there was significant in plate thickness, plate porosity and percent bone in some subregions (mostly AS and PS) between NoOA and OA groups (Fig.9).

In subchondral bone trabeculae, there was significant intragroup variability detected in mean percent bone volume between subregions of OA and no significant difference in NoOA Fig 10. Subchondral trabecular bone intergroup results are illustrated in Fig 11. The difference in subchondral trabecular bone morphological and topological parameters such as BV/TV, Tb.Th, Tb.Pf, FD and DA were statistically significant between NoOA and OA samples for AS and AI subregions, respectively ($P < 0.0001$) (Fig 11 & 12).

Subchondral bone plate intragroup variability

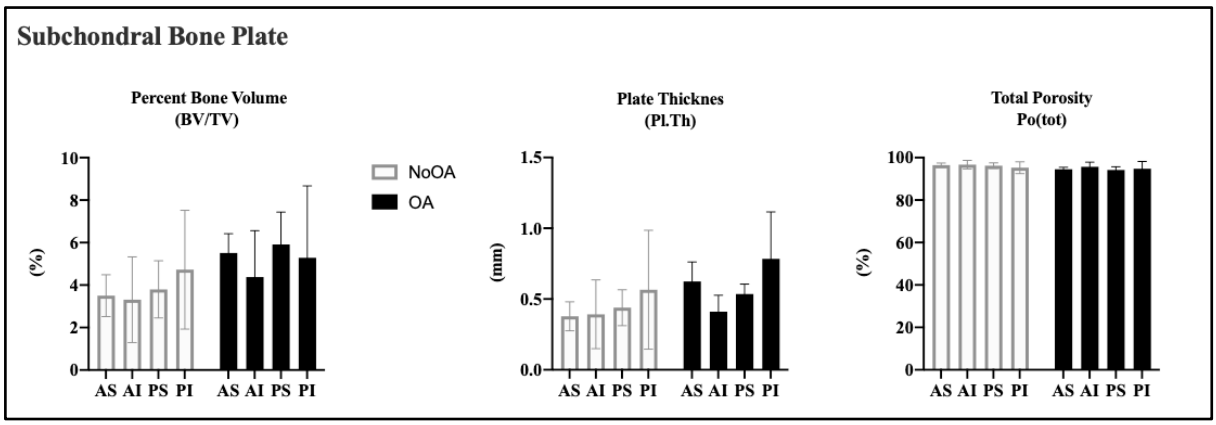

Fig 8. Intragroup variability. Two-way ANOVA results of plate parameters. BV/TV, Pl.Th and T.Po is with non-significant interaction. Data shown as mean ± standard deviation.

Subchondral bone plate intergroup variability

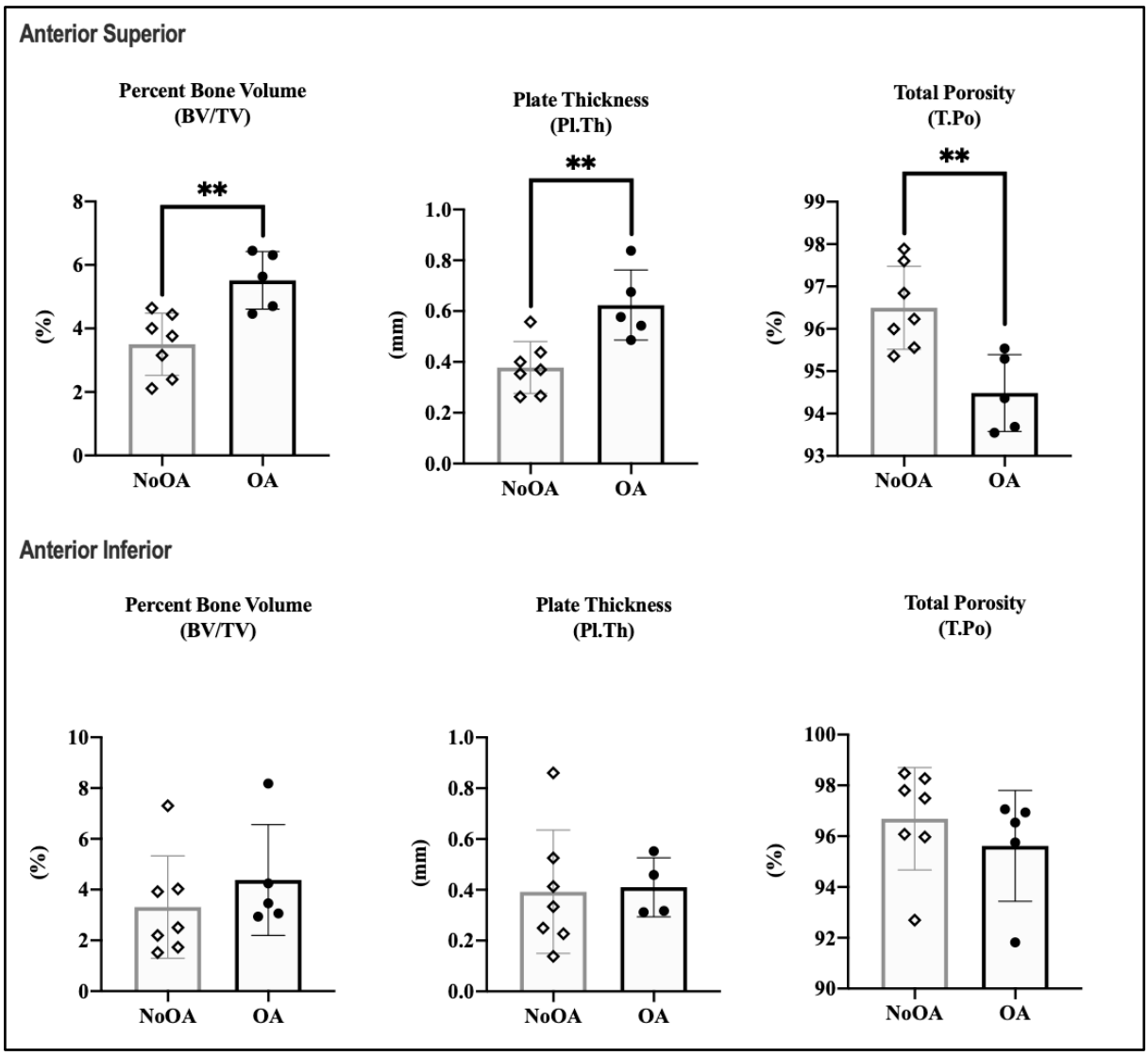

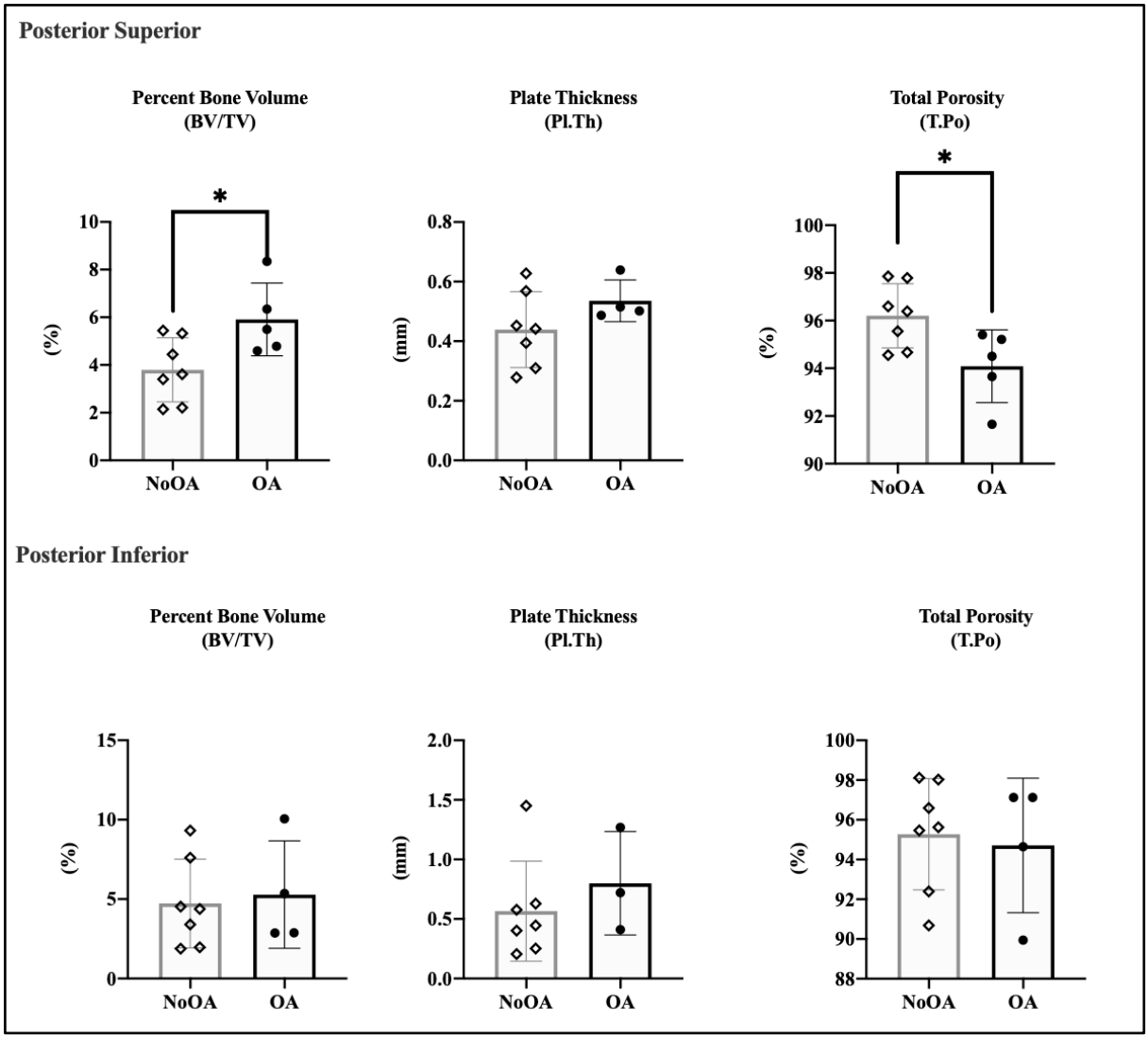

Fig 9. Intergroup variability. Unpaired t-test results of plate parameters. Data shown as mean ± standard deviation, Comparison *P* value $^{*}P < 0.05$, $^{**}P < 0.0001$. BV/TV, Pl.Th,and T.Po are with non-significant difference at AI. Pl.Th is with non-significant difference at PS. BV/TV, Pl.Th and T.Po is with non-significant difference at PI.

Trabecular bone intragroup variability

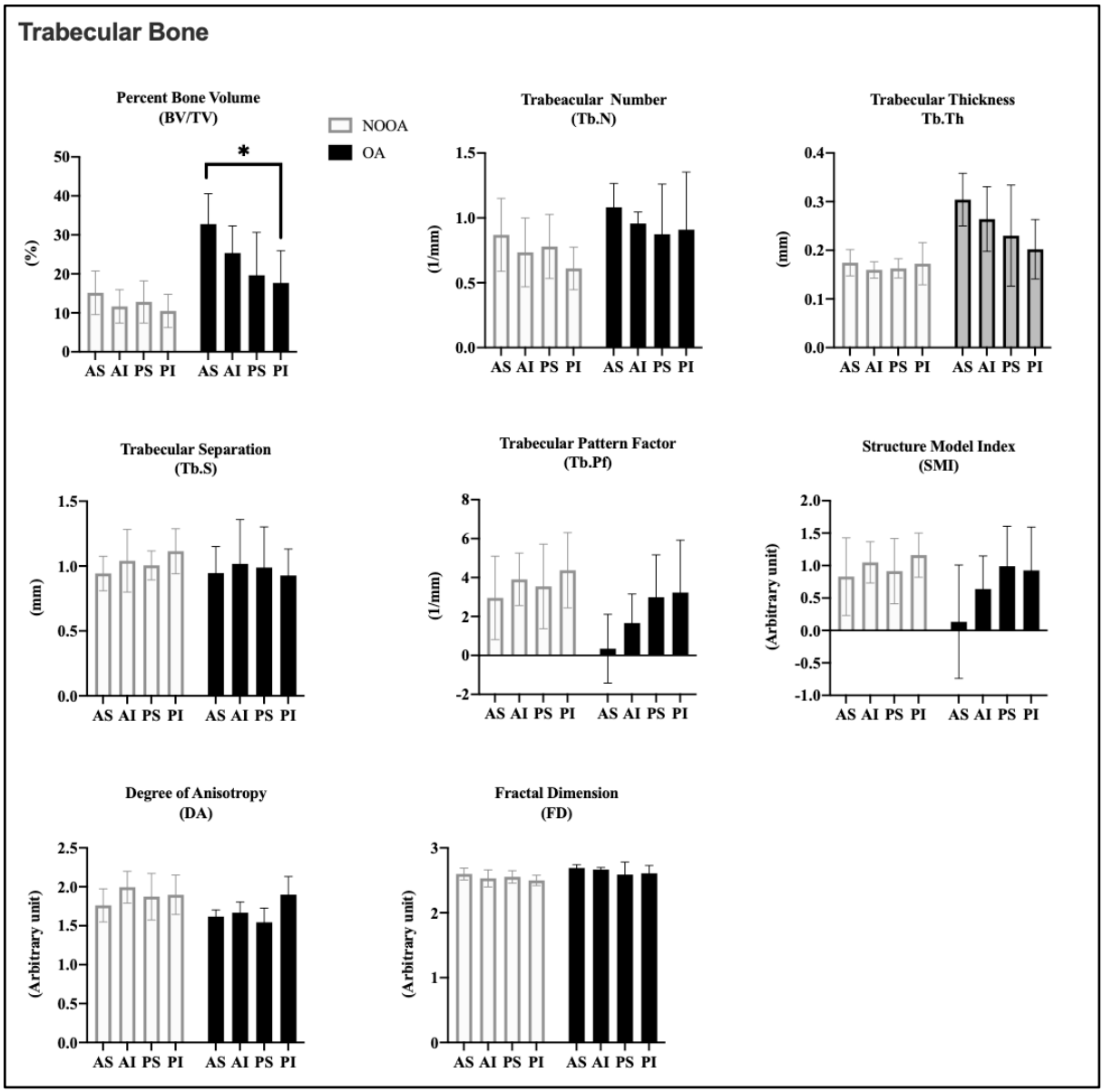

Fig 10. Intragroup variability. Two-way ANOVA results of trabecular bone. Data shown as mean ± standard deviation, Comparison *P* value $^{*}P < 0.05$. Tb.N, Tb.Th, Tb.S, Tb.Pf, SMI, DA and FD is with non-significant interaction.

Trabecular bone intergroup variability

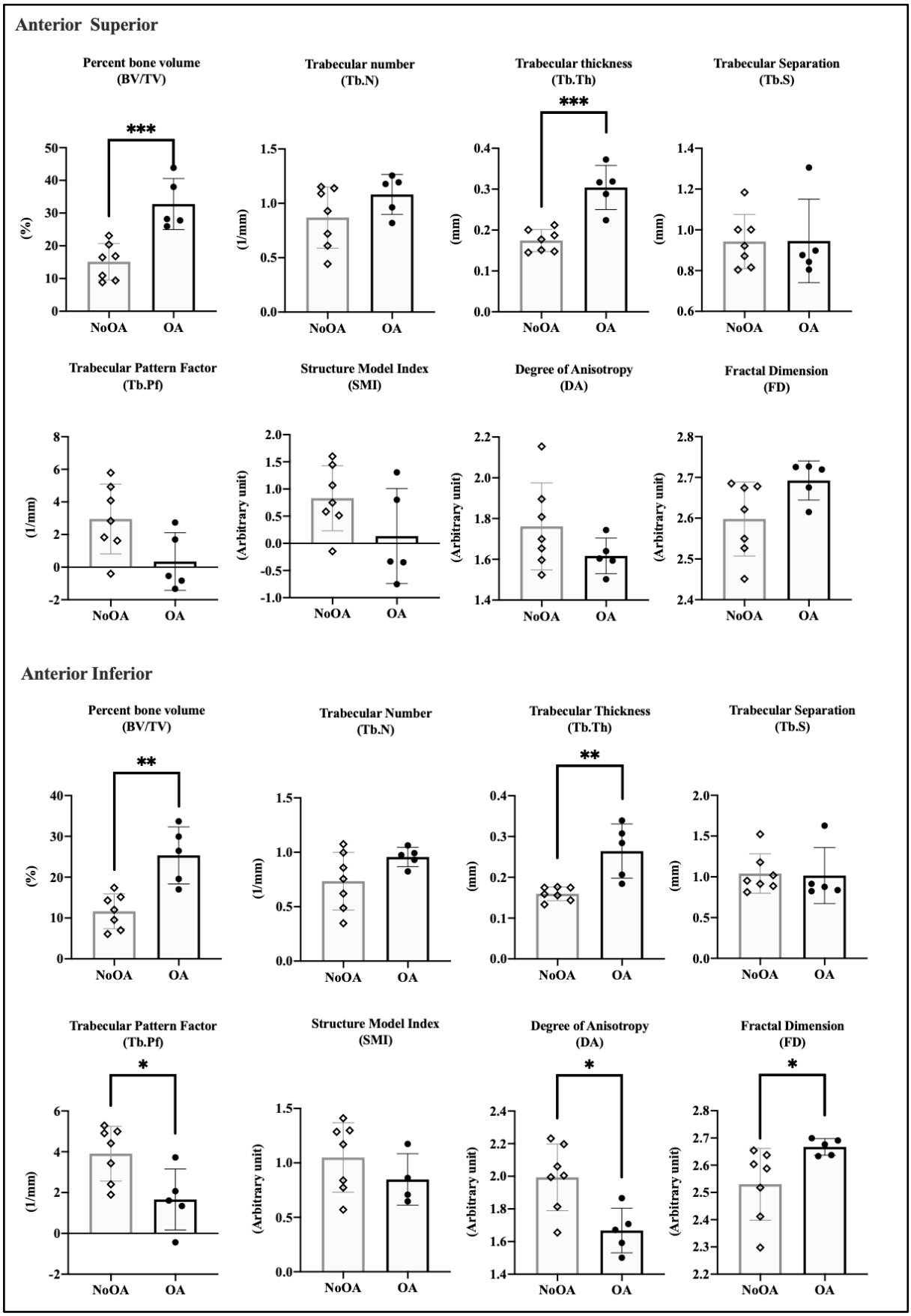

Posterior Superior

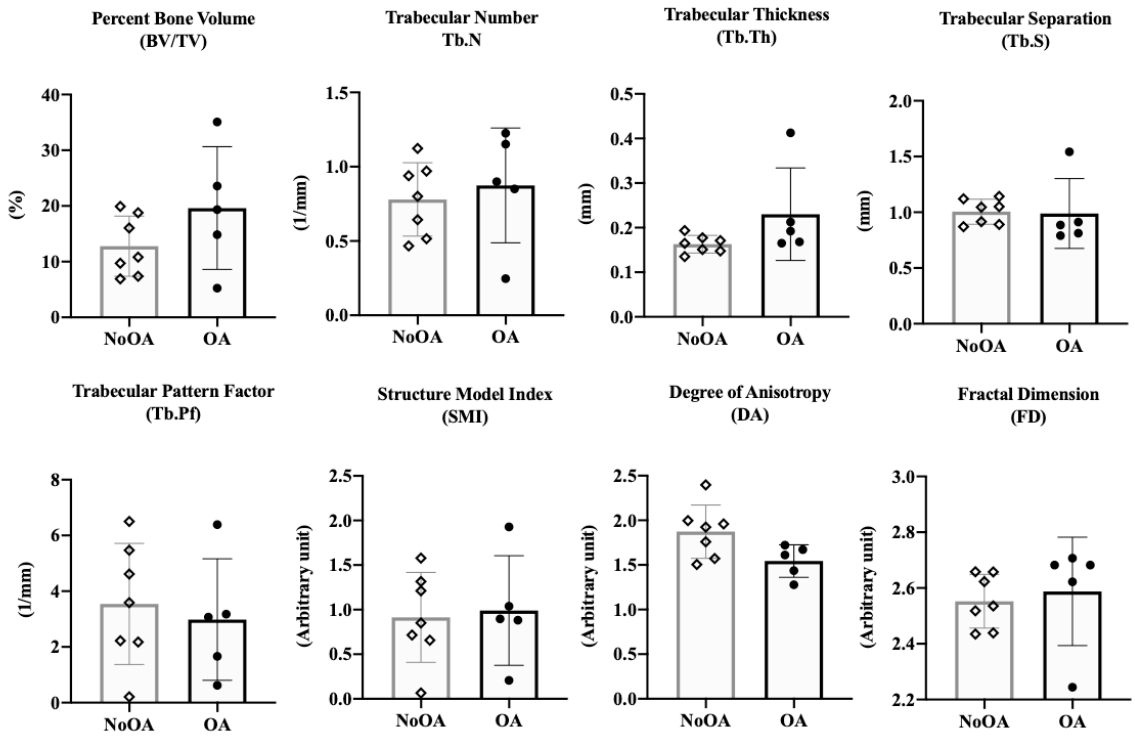

Posterior Inferior

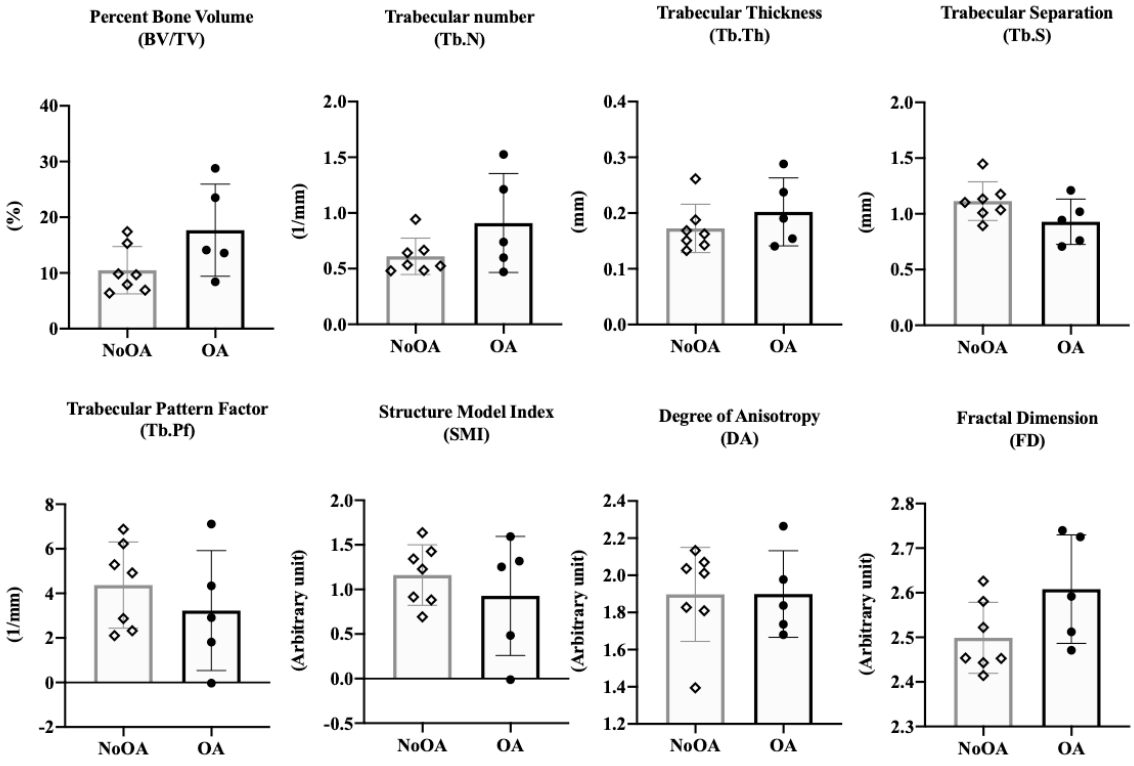

Fig 11. Difference between groups. Unpaired t-test results of trabecular bone parameters in anterior superior, anterior inferior, posterior superior and posterior inferior regions. Data shown as mean ± standard deviation. Comparison *P* value **P* < 0.05, ***P* < 0.001, ****P* <0.0001.

Trabecular bone

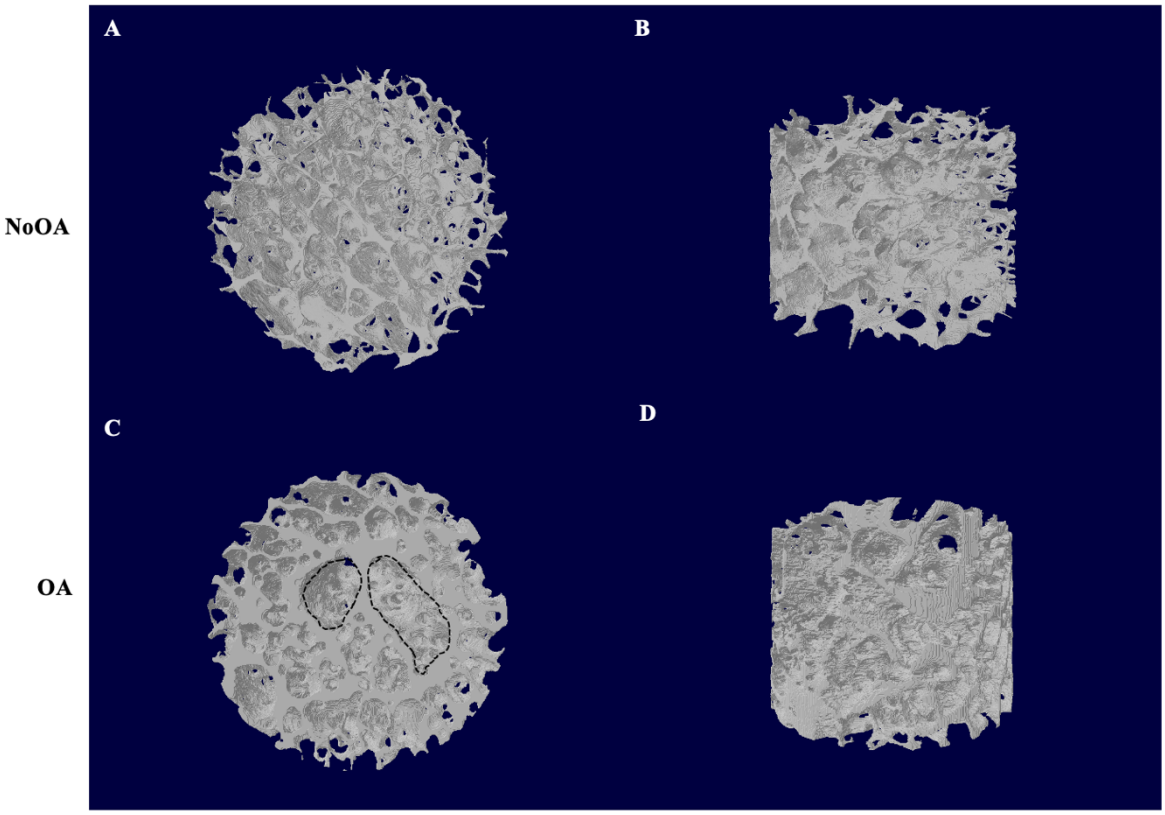

Fig 12. Micro-CT 3D models of trabecular bone for NoOA (A-B) and OA (C-D) in AS region with higher BV/TV and thickened trabecular and two cysts marked by black pattern.

Synchrotron micro-CT assessment

First, we performed an intragroup analysis to investigate if there was a difference in vascular canal parameters between anatomical regions (Fig 13). We did not find the statistically significant difference within NoOA, but in OA, R.Vas.S/BV was different between NoOA and OA subregions. Then we compared anatomical regions between OA and NoOA (Fig 14). In the AS region, we found that Vas.Dn is increased in OA group. In AI region, Vas.V and Vas.Dm were significantly increased in OA

compared to NoOA group (P <0.04). In PS region, we did not find any difference between OA and NoOA groups, but there was a significant decrease in Vas.V in OA compared to NoOA (Fig 14).

Intragroup analysis indicated that there is no significant difference in osteocyte lacunar morphological and topological parameters between regions in both NoOA and OA groups (Fig 15). Additionally comparing regions between NoOA and OA, no statistically significant difference was found except La.Dn (P = 0.03) in PS region (Fig 16).

Vascular canal intragroup variability

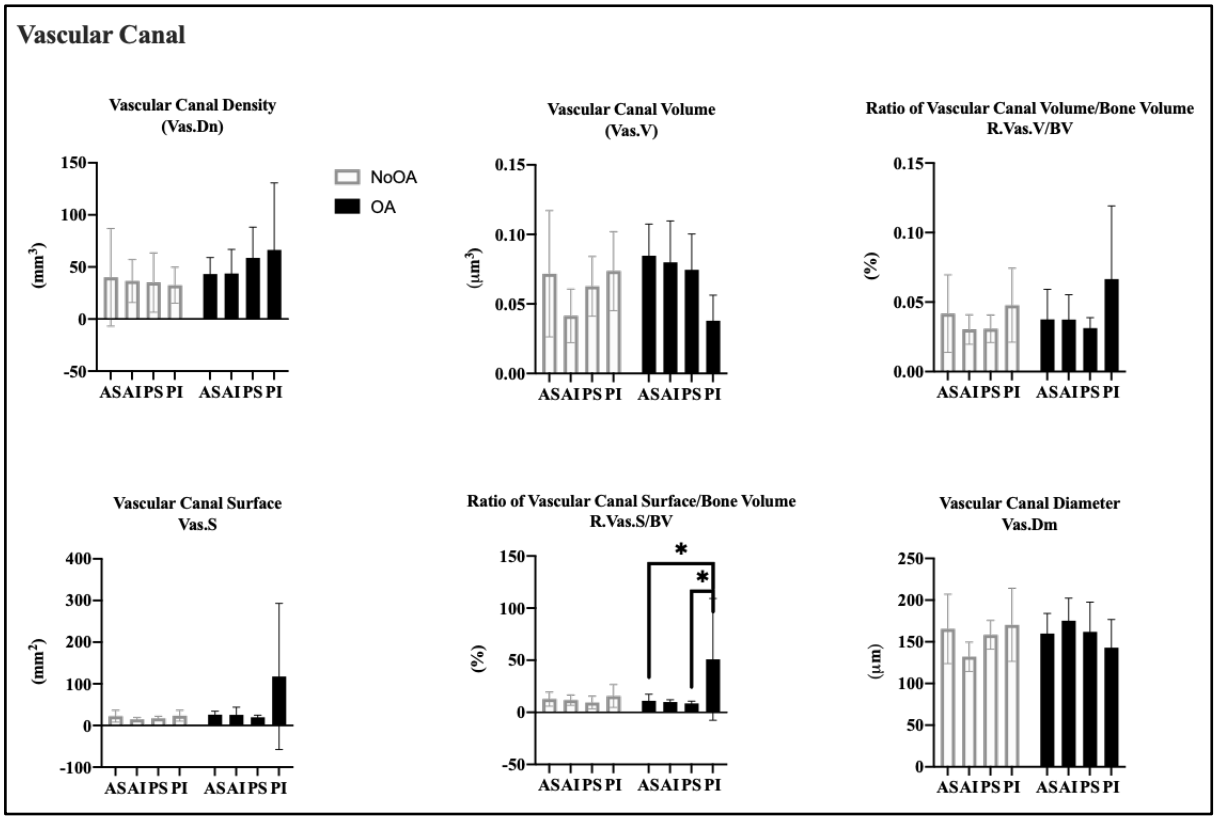

Fig 13. Intragroup variability. Two-way ANOVA results of vascular canal parameters. Data shown as mean ± standard deviation, Comparison *P* value $^{*}P < 0.05$. Vas.Dn, Vas.V, R.Vas.V/BV, Vas.S and Vas.Dn was with non-significant interaction.

Vascular canal intergroup variability

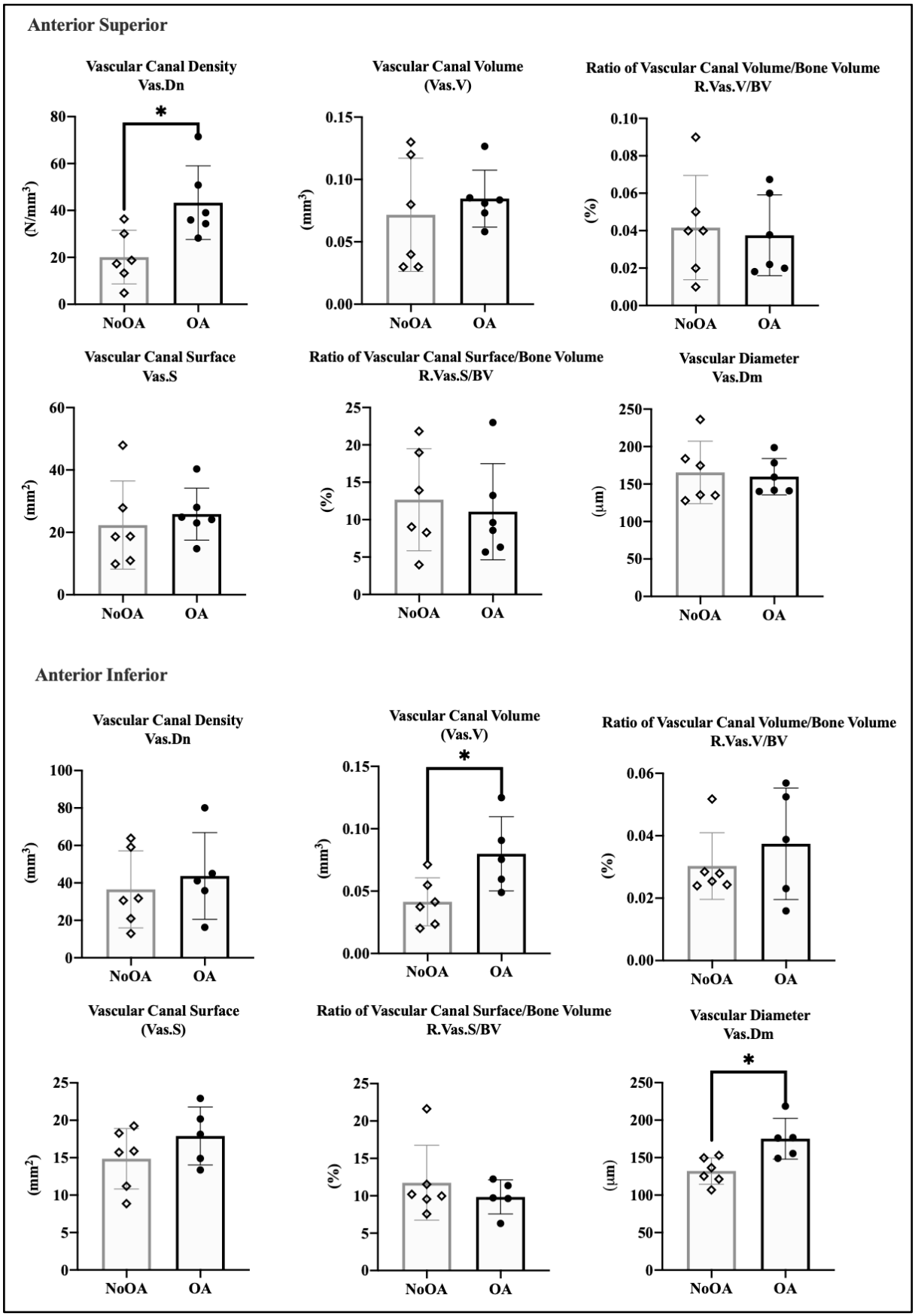

Posterior Superior

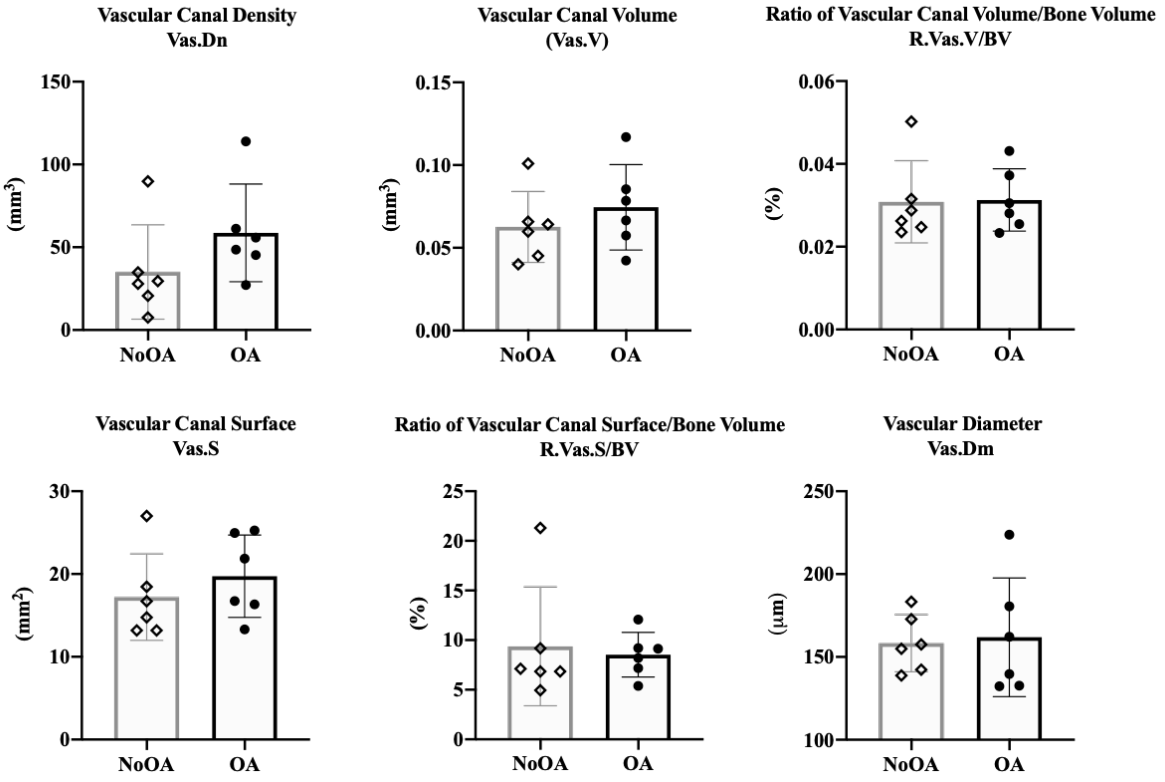

Posterior Inferior

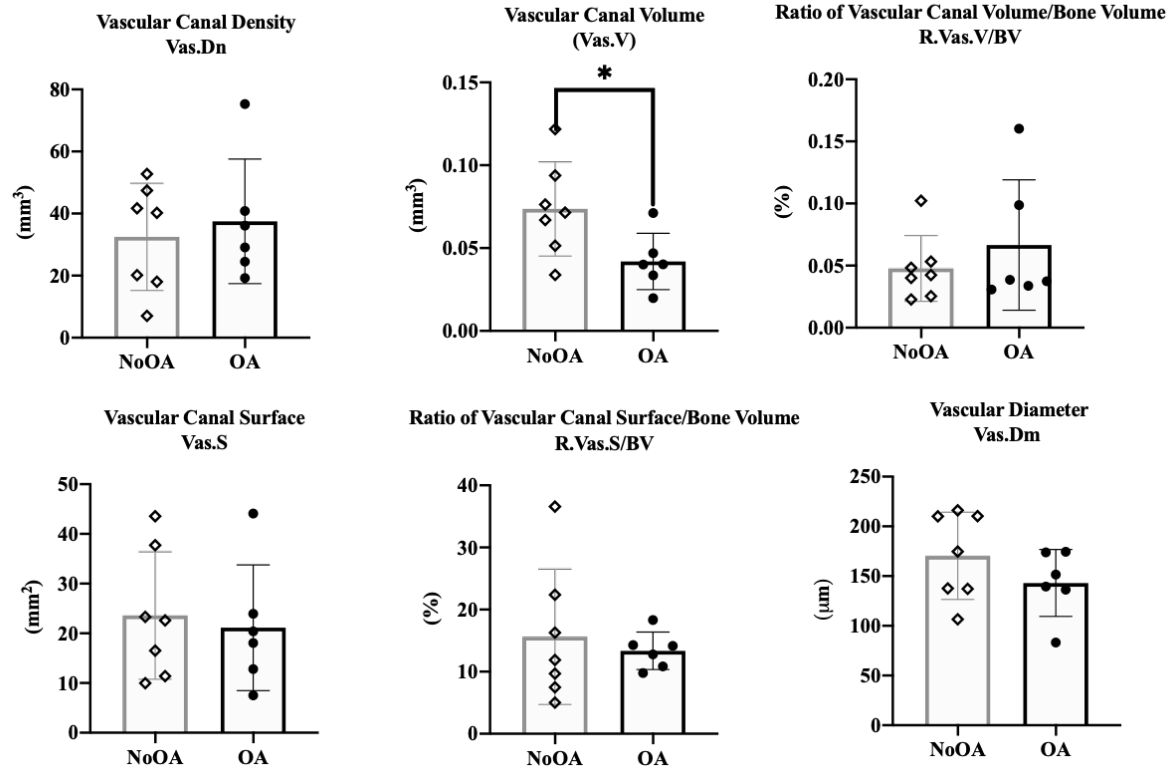

Fig 14. Difference between groups. Unpaired t-test results of vascular canal parameters in anterior superior, anterior inferior, posterior superior and posterior inferior regions. Data shown as mean ± standard deviation. Comparison *P* value $*P < 0.05$.

Osteocyte lacunar intragroup variability

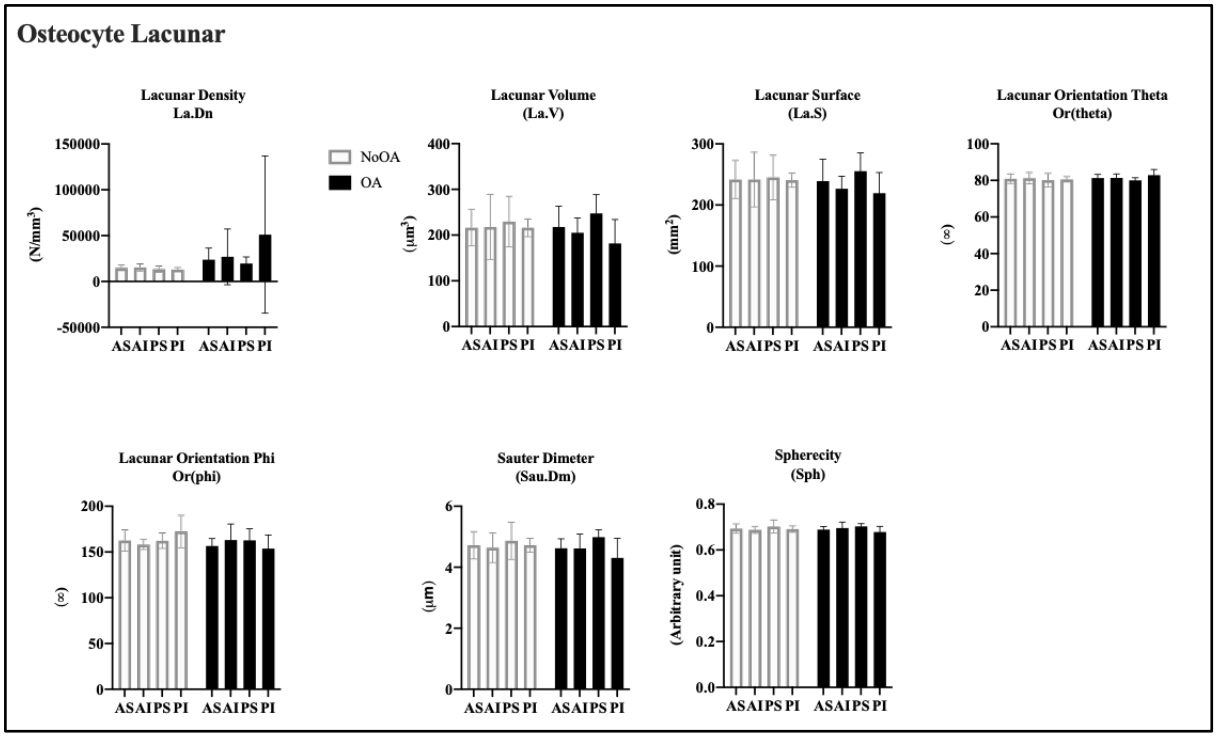

Fig 15. Intragroup variability. Two-way ANOVA results of osteocyte lacunar parameters. All parameters were with non-significant interaction. Data shown as mean ± standard deviation.

Osteocyte lacunar intergroup variability

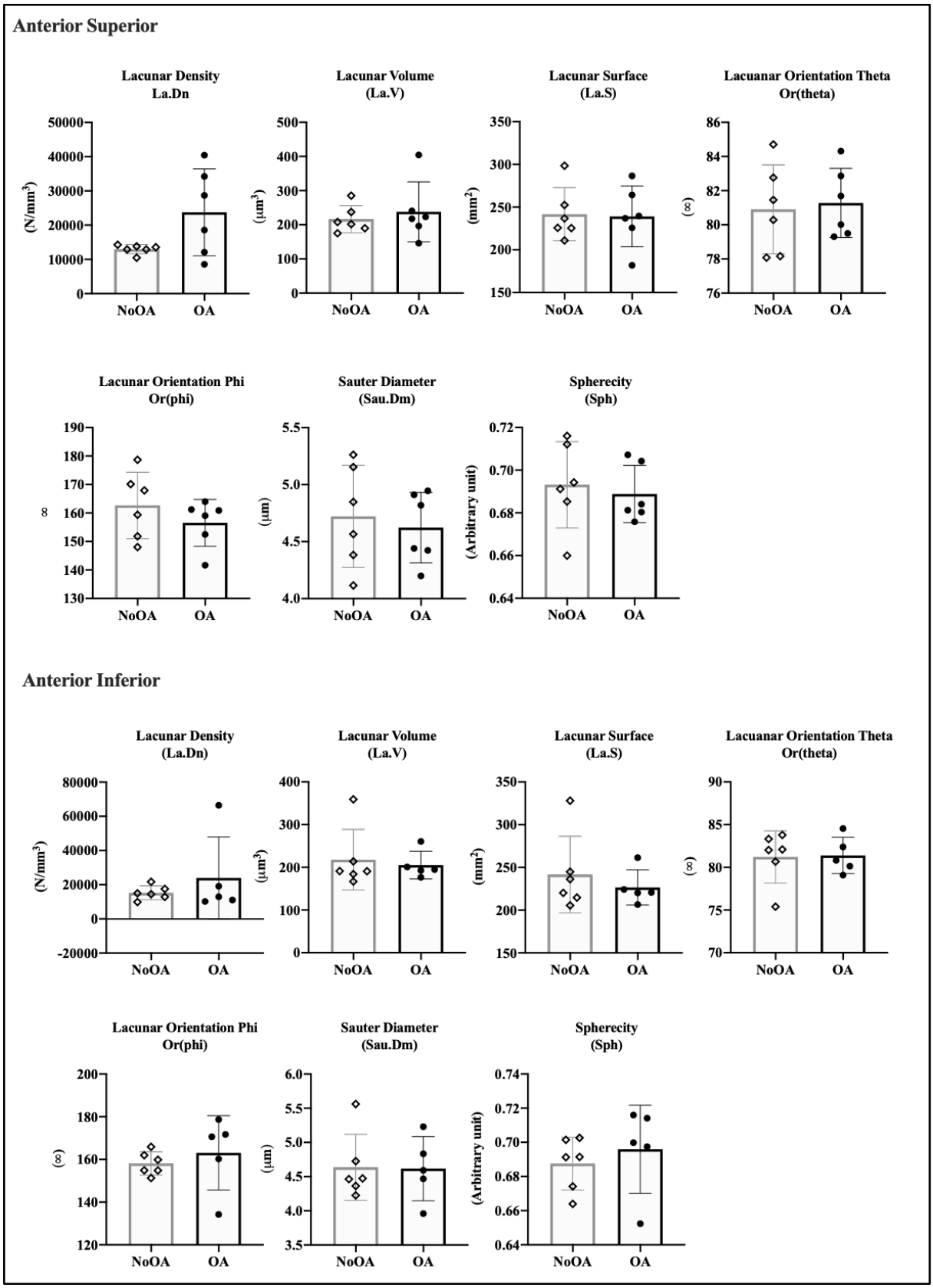

Posterior Superior

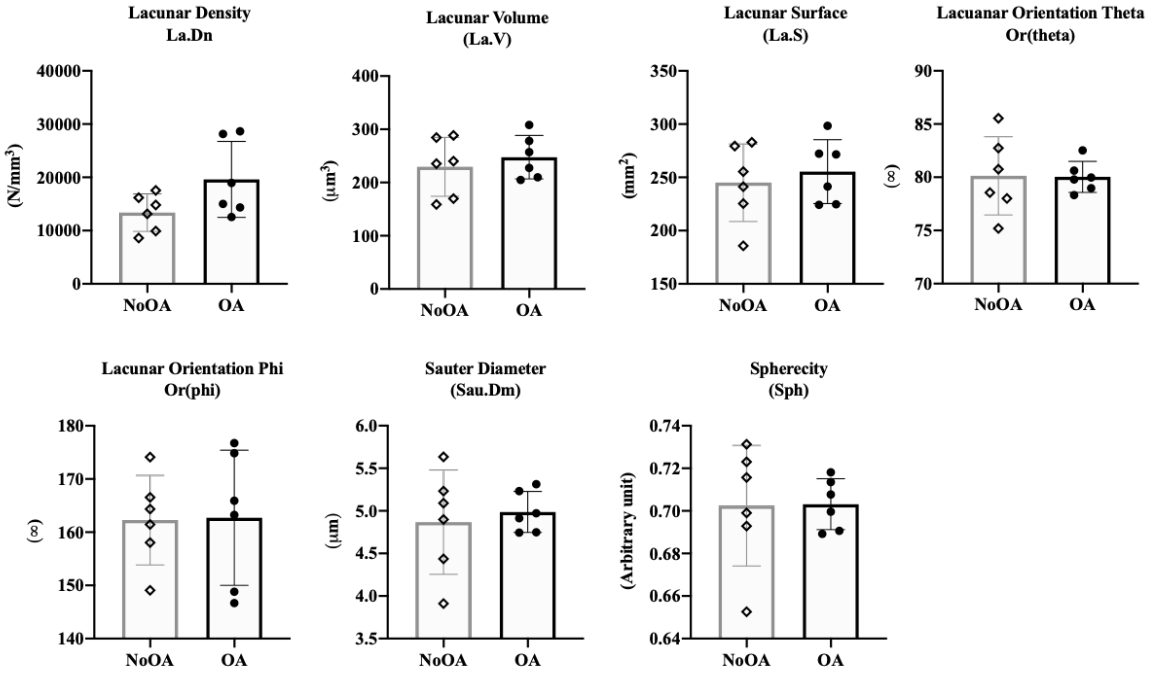

Posterior Inferior

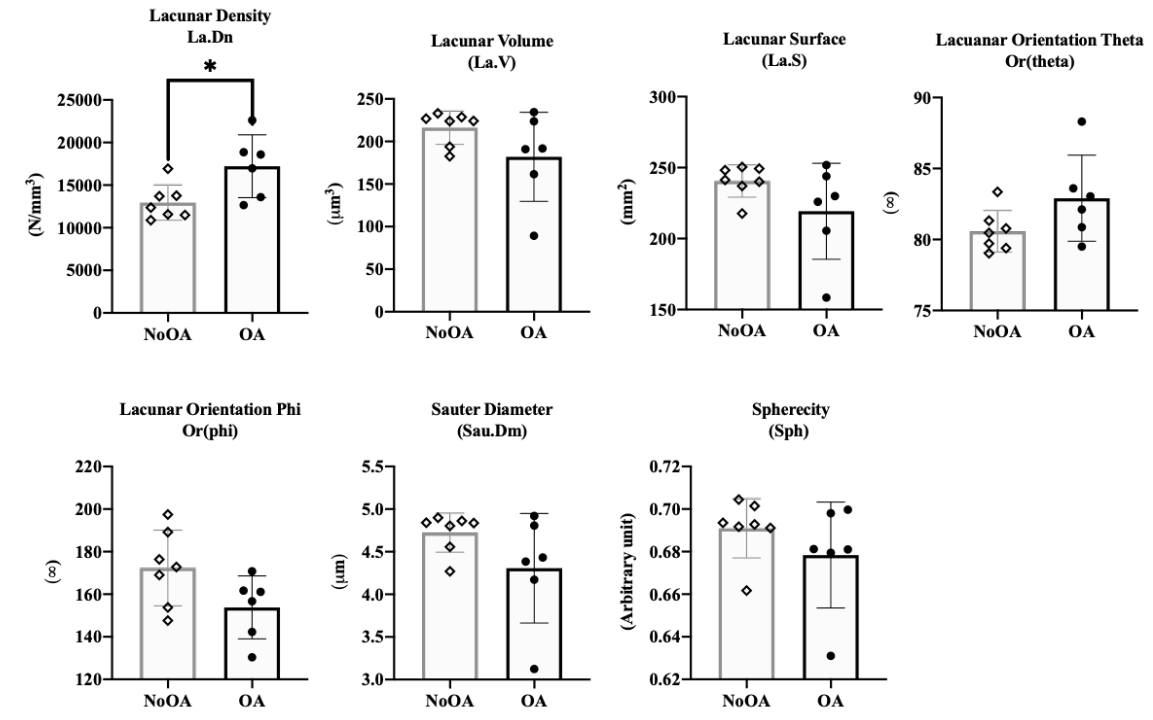

Fig 16. Difference between groups. Unpaired t-test results of osteocyte lacunar parameters in anterior superior, anterior inferior, posterior superior and posterior inferior regions. Data shown as mean ± standard deviation. Comparison *P* value $*P < 0.05$.

Qualitative analysis for vascular canals and osteocyte lacunar

Anterior superior

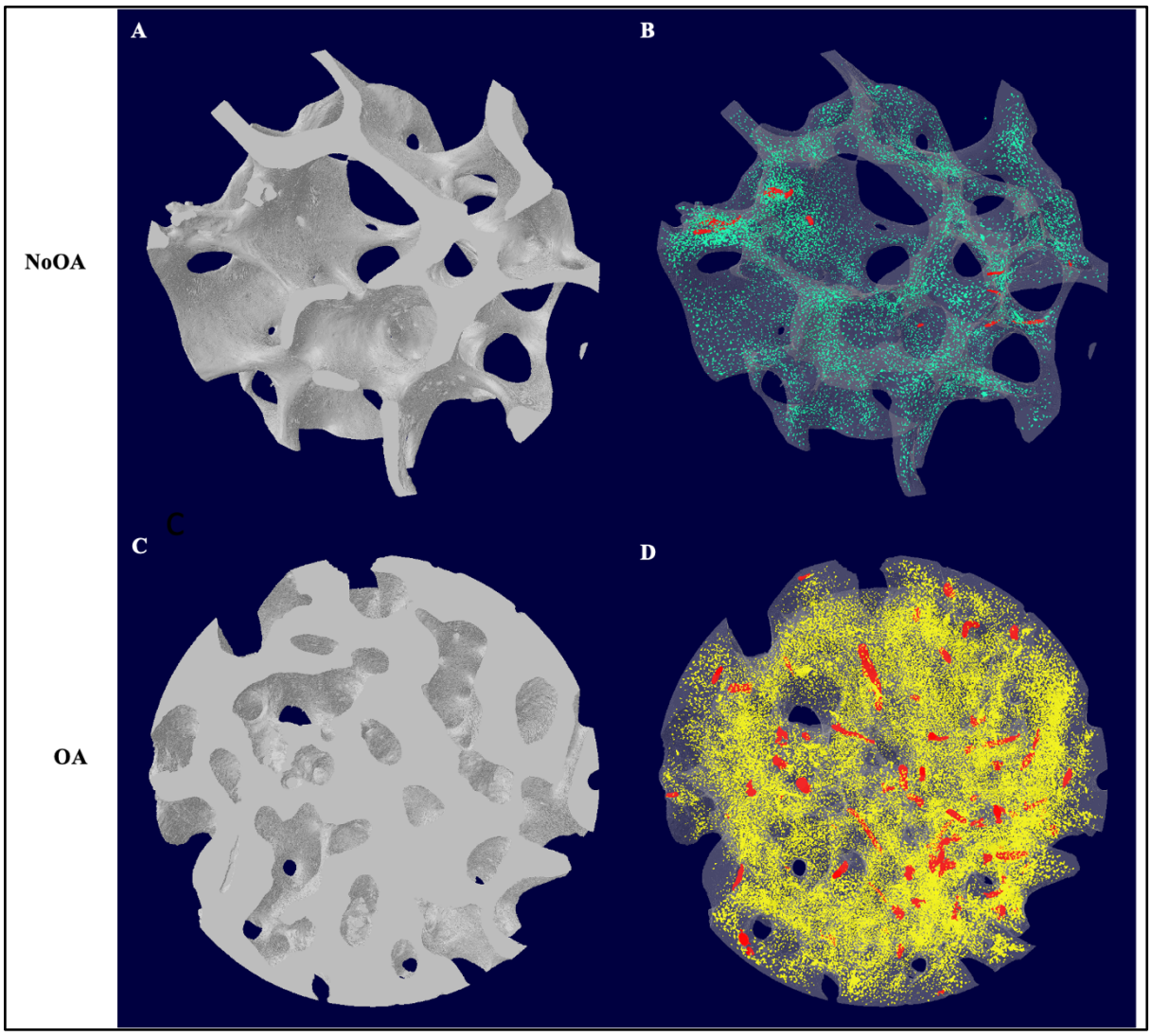

Anterior inferior

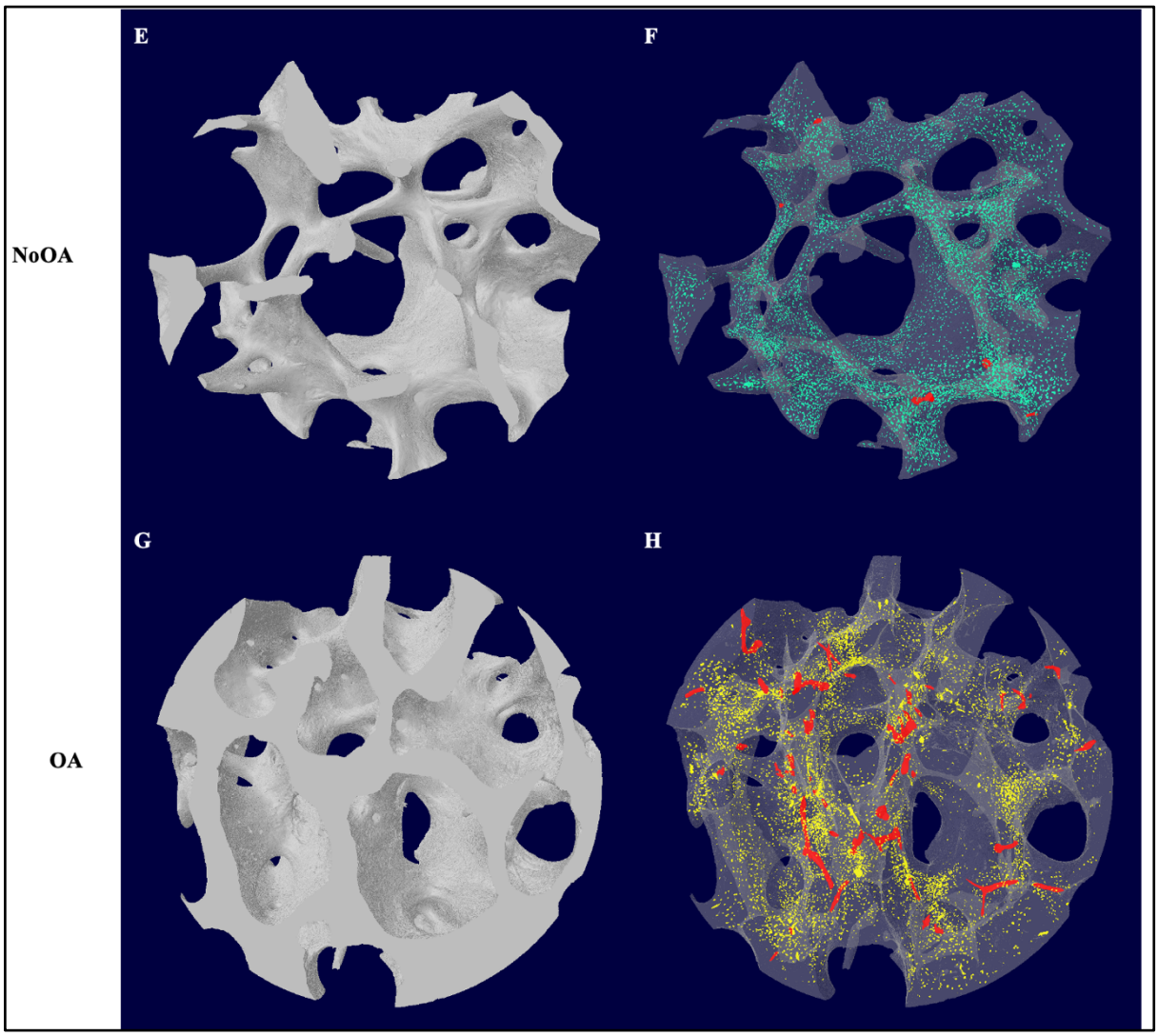

Posterior superior

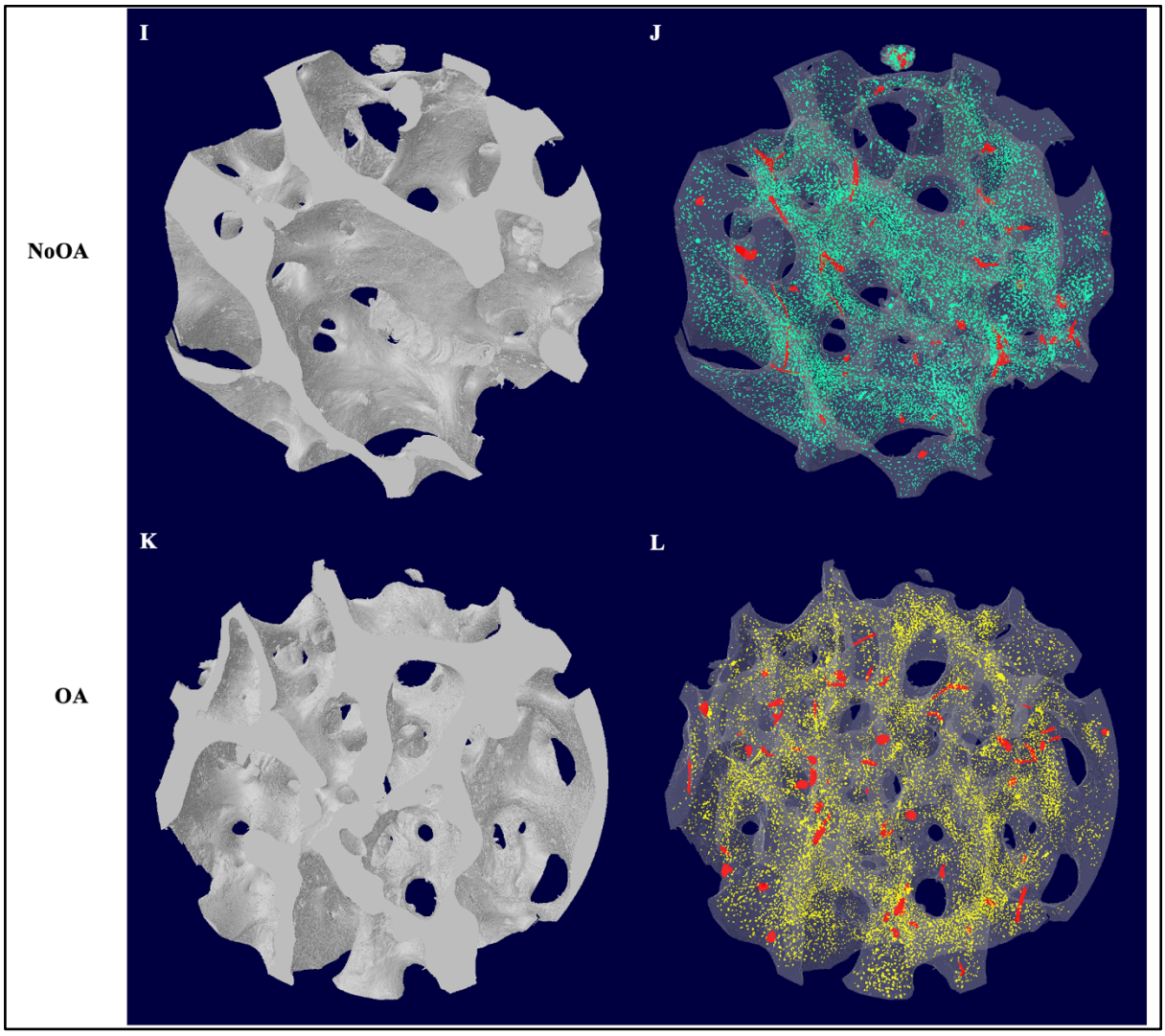

Posterior inferior

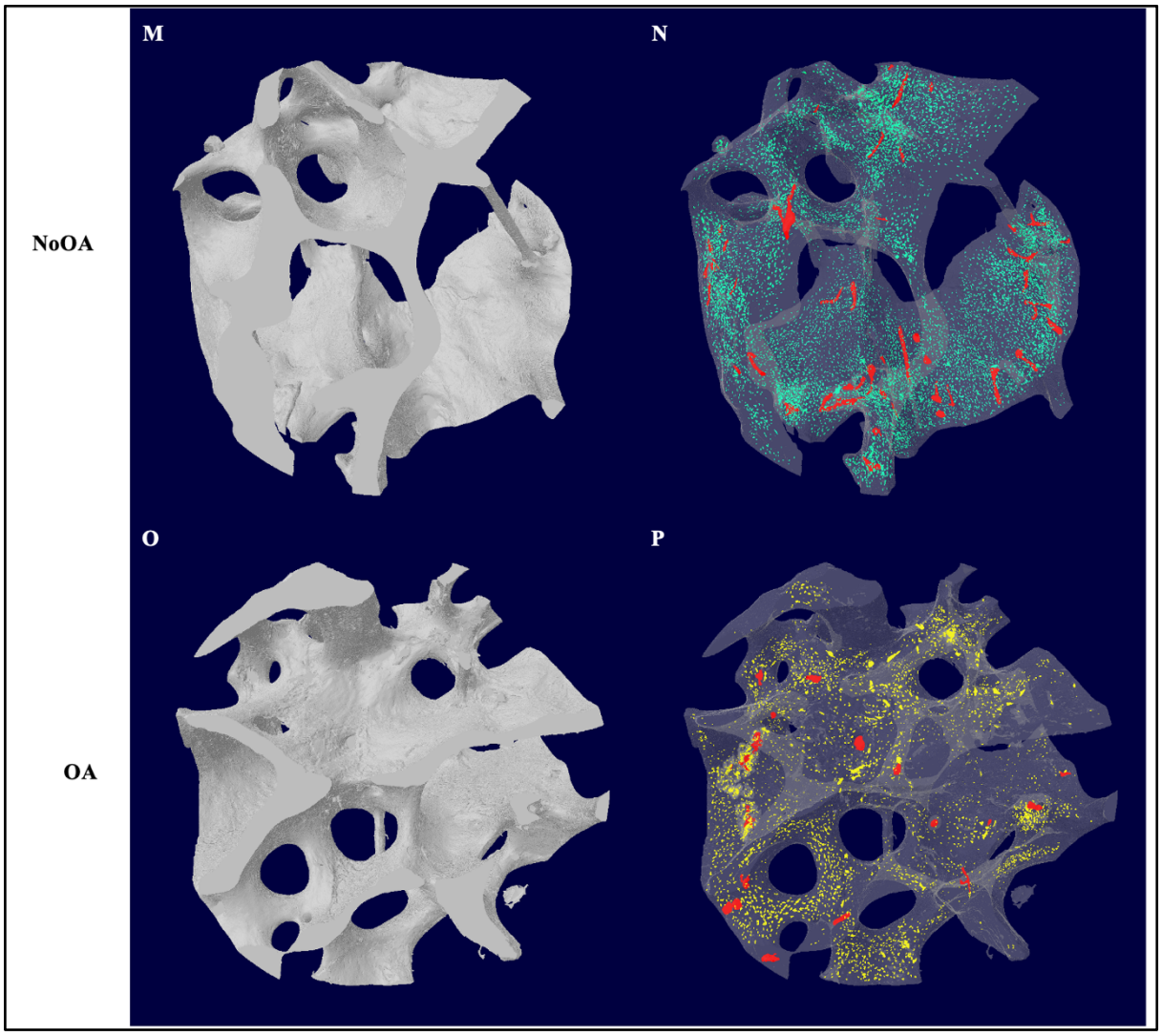

Fig 17. Synchrotron micro-CT 3D models showing trabecular bone white and transparent (A-P), vascular canals (red) (A-P) and osteocyte lacunar for NoOA (green - B, F, J & N) and OA (yellow – D, H, L & P).

DISCUSSION

This is the first study describing comprehensively subchondral bone microstructure (subchondral plate and trabeculae), vascularisation of bone matrix in 4 different anatomical regions and osteocyte lacunae properties and comparing it between NoOA and OA. We observed that subchondral bone pathologies visualised by MRI (BMLs and cysts) occurred mainly in bone (anterior regions) beneath areas where cartilage has depleted, resulting in changes in the plate and trabecular bone micro-architecture. These data suggest that there is an association between subchondral bone alterations and the presence of BMLs and cysts in the OA group. However, there was no significant difference in NoOA group for parameters describing subchondral bone microstructure.

Structural differences in the subchondral bone plate and trabeculae in hip OA patients

Most of the microstructural differences were found in the anterior regions of the femoral head known to be associated with lower bone quality due to higher peak forces and the presence of pathologies[48-51].

Subchondral bone plate

Higher subchondral bone volume fraction and plate thickness in the OA group suggested hip OA was in the late stage, which is in line with previous studies[25, 52, 53]. These bone changes seem to signify the adaptive mechanism (modelling and remodelling) of subchondral bone architecture as a result of cartilage loss and the impact of mechanical loading or biomechanical influence reported in previous studies[54-56]. With increasing plate thickness, total plate porosity in the OA group decreased compared with NoOA, which contradicts a study by Li et al.[53] who found increased plate porosity with increased plate thickness in advanced OA. The increased porosity in NoOA group could be due to regular bone changes associated with aging, which was reported by a study investigating age-related changes in human trabecular microarchitecture[57].

Subchondral trabeculae

Within the OA group, the AS region had increased bone volume compared to the PS region. However, comparing NoOA and OA, there was a 14% increase in mean bone volume fraction and trabecular bone

thickness in OA was twice that of NoOA in two regions (AS and AI). These data are supported by previous studies that found increased BV/TV and Tb.Th in corresponding femoral head locations[26, 51, 53] to be associated with large cyst number and volume[58]. Furthermore, higher cyst number and volume was associated with future joint replacement[59, 60]. Some studies found that multiple subchondral cysts, which are sometimes colocalised with subchondral BMLs[61] occurring at the superior weight-bearing surface of the femoral head[62] were associated with higher BV/TV and Tb.Th and related to an increase in bone density and hardening (sclerosis) [11, 59]. Chiba et al.,[59] suggested that each cyst caused reactive bone formation itself, and the multiple formations of such reactive bone lead to bone sclerosis or perhaps cyst formation changes the distribution of mechanical load in the subchondral bone resulting in more stress on the remaining trabecular bone followed by bone sclerosis[59]. However, the mechanism of the subchondral cyst and sclerosis formation is still unclear[11, 59]

Trabecular number and separation did not increase between OA and NoOA groups in all regions. Trabecular bone structures were more plate-like due to low structure model index and were less connected as a result of higher mean value of the trabecular pattern factor, in the AI region. What is more, the degree of anisotropy in trabeculae was higher in AI for NoOA compared to OA group, because it has been suggested to be more sensitive to aging and trabecular bone changes[57]. Increased fractal dimension in OA suggests trabecular bone surface was less smooth associated with advance OA[63].

Regarding BMLs, it is also believed to occur in regions with the highest loading. BMLs in the anterior region (area with the highest pressure) of the femoral head was associated with cartilage volume loss[64] and subsequent sclerosis[29, 65]. This seems to support the altered bone microarchitecture found in the anterior region of this study. Studies have suggested that BMLs may be present before clinical symptoms (pain), and add that unresolved BMLs coupled with persistent joint loading results in increased fibrosis and vascularity[65, 66]. However, little is known about the underlying mechanism of BMLs formation[50, 66].

This study explored both BMLs and cysts in the OA femoral head and found they occurred at anterior regions, where the aforementioned subchondral bone alterations were recorded. Thus, suggesting its possible role in bone sclerosis reported in other studies[26].

Vascular canal and osteocyte lacunar in trabeculae

Vascular canal

The changes in OA vascular canals in this study likely suggest its role in subchondral bone remodelling, evidently seen in the subchondral plate and trabecular bone volume and thickness. These data are supported by previous studies which found increased angiogenesis in the osteochondral unit in OA patients with subchondral pathology[39, 40]. Subchondral angiogenesis has also been shown to be closely associated with nerve growth, which is responsible for the manifestation of the clinical symptoms (pain) in individuals with pathology (BMLs and cysts) in hip OA[67]. The decrease in vascular canal volume in the PI region may suggest lower remodelling in the region. However, there is lack of data on the regional variation of vascular canal in hip OA. Therefore, comparison to other studies could not be made. Tiede et al.[38] have reported the intimate connection of vascular canals with osteocyte lacunar through dendritic processes in canaliculi (narrow tunnels) that carries signalling factors and nutrients to and from the osteocytes[38].

Osteocyte lacunar

Osteocytes represent about 90% of bone cells and are located in lacunae (space), interconnected with other osteocytes to form a network in the bone matrix. They are believed to act as mechanosensory cells, which translate mechanical force (compressive) into biochemical signals via dendritic processes and coordinate the osteoclasts and osteoblasts for bone resorption and formation respectively[37, 38]. Human bone studies have found a correlation between dense osteocyte network and more desirable bone tissue quality[68]. Moreover, robust osteocyte network has been suggested to be vital in the initiation of remodelling responses and opposing structural damage to uphold healthy and mechanically resilient bone[69]. This is in line with studies that suggest differences in lacunar properties are linked with the functional adaptation of bone[70-72]. In this current study, it cannot be excluded that the small sample size might have resulted in the parameters not reaching statistical significance. Another reason could be differences in methodology in the evaluation of osteocyte lacunar parameters. For instance, some of these studies were performed in animals using 2D analysis, and even those performed in humans had samples collected from different anatomical regions believed to have different osteocyte distribution, shape and size[73]. All of which could make the increase in lacunar density in the OA group at the PI region significantly weak even though it might be in line with studies reported in Mader et al.,[73] study.

The strength of this cross-sectional study relates to the comprehensive analysis of the subchondral bone microarchitecture using micro-CT coupled with a novel higher spatial resolution synchrotron micro-CT. There are several limitations to this study. Firstly, the small sample size was used in this study because some images had unknown pathologies, which led to the exclusion of these specimens and a further reduction in sample size. Thus, it limits the generality of the results. Therefore, a larger sample size will be required in future studies to achieve the aims of this study. Secondly, due to the cross-sectional design of this study, the genesis of BMLs and cysts were not identified, and the early stage of the disease could not be confirmed in the subchondral bone structure. Moreover, localised cartilage volume was not calculated for each anatomical region, hence, making it difficult to determine whether pathology presence was secondary to cartilage volume loss or vice versa. What is more, the

quantification of osteocyte lacunae did not consider the presence/absence of viable and non-viable osteocytes.

In conclusion, this study showed that degenerated cartilage or, the presence of MRI bone pathology BML or cyst or both might contribute to alteration in subchondral bone microarchitecture in hip OA and drive the disease progression. Hence, BMLs and cysts could be monitored with advanced MRI imaging technique for disease progression in hip OA patients.

PROFESSIONAL AND FUNDING ACKNOLEDGEMENT

Professor David Findlay

Dr Julia Kuliwaba

Dr Dzenta Muratovic

Dr Ryan Quarrington

Dr Agatha Labrinidis

Funding from International Synchrotron Access Program (Switzerland)

National Health and Medical Research Council Australia

REFERENCES

1. Guymer E, Baranyay F, Wluka AE, Hanna F, Bell RJ, Davis SR, Wang Y & Cicuttini FM (2007). A study of the prevalence and associations of subchondral bone marrow lesions in the knees of healthy, middle-aged women. *Osteoarthritis Cartilage* **15**, 1437-42.
2. Dagenais S, Garbedian S & Wai EK (2008). Systematic Review of the Prevalence of Radiographic Primary Hip Osteoarthritis. *Clinical Orthopaedics and Related Research* **467**, 623.
3. Martel-Pelletier J, Barr AJ, Cicuttini FM, Conaghan PG, Cooper C, Goldring MB, Goldring SR, Jones G, Teichtahl AJ & Pelletier JP (2016). Osteoarthritis. *Nature Reviews Disease Primers* **2**, 18.
4. Aho OM, Finnila M, Thevenot J, Saarakkala S & Lehenkari P (2017). Subchondral bone histology and grading in osteoarthritis. *Plos One* **12**, 16.
5. Taruc-Uy RL & Lynch SA (2013). Diagnosis and treatment of osteoarthritis. *Prim Care* **40**, 821-36, vii.
6. Castaneda S, Roman-Blas JA, Largo R & Herrero-Beaumont G (2012). Subchondral bone as a key target for osteoarthritis treatment. *Biochem Pharmacol* **83**, 315-23.
7. Hunter DJ & Bierma-Zeinstra S (2019). Osteoarthritis. *Lancet* **393**, 1745-1759.
8. Braun HJ & Gold GE (2012). Diagnosis of osteoarthritis: imaging. *Bone* **51**, 278-88.
9. Radin EL & Rose RM (1986). Role of subchondral bone in the initiation and progression of cartilage damage. *Clinical Orthopaedics and Related Research* **No. 213**, 34-40.
10. Botter SM, van Osch GJ, Waarsing JH, van der Linden JC, Verhaar JA, Pols HA, van Leeuwen JP & Weinans H (2008). Cartilage damage pattern in relation to subchondral plate thickness in a collagenase-induced model of osteoarthritis. *Osteoarthritis Cartilage* **16**, 506-14.
11. Chiba K, Ito M, Osaki M, Uetani M & Shindo H (2011). In vivo structural analysis of subchondral trabecular bone in osteoarthritis of the hip using multi-detector row CT. *Osteoarthritis and Cartilage* **19**, 180-185.

12. Henrotin Y, Pesesse L & Sanchez C (2009). Subchondral bone in osteoarthritis physiopathology: state-of-the art and perspectives. *Biomed Mater Eng* **19**, 311-6.

13. Bijlsma JW, Berenbaum F & Lafeber FP (2011). Osteoarthritis: an update with relevance for clinical practice. *Lancet* **377**, 2115-26.

14. Ackerman IN, Pratt C, Gorelik A & Liew D (2018). Projected Burden of Osteoarthritis and Rheumatoid Arthritis in Australia: A Population-Level Analysis. *Arthritis Care Res (Hoboken)* **70**, 877-883.

15. Brandt KD, Fife RS, Braunstein EM & Katz B (1991). Radiographic grading of the severity of knee osteoarthritis: Relation of the Kellgren and Lawrence grade to a grade based on joint space narrowing, and correlation with arthroscopic evidence of articular cartilage degeneration. *Arthritis and Rheumatism* **34**, 1381-1386.

16. Kijowski R, Blankenbaker D, Stanton P, Fine J & Smet A (2006). Correlation between radiographic findings of osteoarthritis and arthroscopic findings of articular cartilage degeneration within the patellofemoral joint. *Skeletal Radiology* **35**, 895-902.

17. Blum A, Raymond A & Teixeira P (2015). Strategy and optimization of diagnostic imaging in painful hip in adults. *Orthop Traumatol Surg Res* **101**, S85-99.

18. Barr AJ, Campbell TM, Hopkinson D, Kingsbury SR, Bowes MA & Conaghan PG (2015). A systematic review of the relationship between subchondral bone features, pain and structural pathology in peripheral joint osteoarthritis. *Arthritis Res Ther* **17**, 228.

19. Ahedi HG, Aitken DA, Blizzard LC, Ding CH, Cicuttini FM & Jones G (2016). Correlates of Hip Cartilage Defects: A Cross-sectional Study in Older Adults. *J Rheumatol* **43**, 1406-12.

20. Nieminen MT, Casula V, Nevalainen MT & Saarakkala S (2019). Osteoarthritis year in review 2018: imaging. *Osteoarthritis and Cartilage* **27**, 401-411.

21. Kumar D, Wyatt CR, Lee S, Nardo L, Link TM, Majumdar S & Souza RB (2013). Association of cartilage defects, and other MRI findings with pain and function in individuals with mild-moderate radiographic hip osteoarthritis and controls. *Osteoarthritis Cartilage* **21**, 1685-92.

22. Rhaney K & Lamb DW (1955). The cysts of osteoarthritis of the hip; a radiological and pathological study. *J Bone Joint Surg Br* **37-b**, 663-75.

23. Ondrouch AS (1963). CYST FORMATION IN OSTEOARTHRITIS. *J Bone Joint Surg Br* **45**, 755-60.

24. Resnick D, Niwayama G & Coutts RD (1977). Subchondral cysts (geodes) in arthritic disorders: pathologic and radiographic appearance of the hip joint. *AJR Am J Roentgenol* **128**, 799-806.

25. Chiba K, Nango N, Kubota S, Okazaki N, Taguchi K, Osaki M & Ito M (2012). Relationship between microstructure and degree of mineralization in subchondral bone of osteoarthritis: a synchrotron radiation microCT study. *J Bone Miner Res* **27**, 1511-7.

26. Inui A, Nakano S, Yoshioka S, Goto T, Hamada D, Kawasaki Y, Egawa H & Yasui N (2013). Subchondral cysts in dysplastic osteoarthritic hips communicate with the joint space: analysis using three-dimensional computed tomography. *Eur J Orthop Surg Traumatol* **23**, 791-5.

27. Dore D, Martens A, Quinn S, Ding C, Winzenberg T, Zhai G, Pelletier JP, Martel-Pelletier J, Abram F, Cicuttini F & Jones G (2010). Bone marrow lesions predict site-specific cartilage defect development and volume loss: a prospective study in older adults. *Arthritis Res Ther* **12**, R222.

28. Xu L, Hayashi D, Roemer FW, Felson DT & Guermazi A (2012). Magnetic Resonance Imaging of Subchondral Bone Marrow Lesions in Association with Osteoarthritis. *Seminars in Arthritis and Rheumatism* **42**, 105-118.

29. Teichtahl AJ, Wang Y, Smith S, Wluka AE, Giles GG, Bennell KL, O'Sullivan R & Cicuttini FM (2014). Structural changes of hip osteoarthritis using magnetic resonance imaging. *Arthritis Res Ther* **16**, 466.

30. Schwaiger BJ, Gersing AS, Lee S, Nardo L, Samaan MA, Souza RB, Link TM & Majumdar S (2016). Longitudinal assessment of MRI in hip osteoarthritis using SHOMRI and correlation with clinical progression. *Seminars in arthritis and rheumatism* **45**, 648-55.

31. Boutry N, Paul C, Leroy X, Fredoux D, Migaud H & Cotten A (2002). Rapidly destructive osteoarthritis of the hip: MR imaging findings. *AJR Am J Roentgenol* **179**, 657-63.

32. Taljanovic MS, Graham AR, Benjamin JB, Gmitro AF, Krupinski EA, Schwartz SA, Hunter TB & Resnick DL (2008). Bone marrow edema pattern in advanced hip osteoarthritis:

quantitative assessment with magnetic resonance imaging and correlation with clinical examination, radiographic findings, and histopathology. *Skeletal Radiol* **37**, 423-31.

33. Maksymowych WP, Cibere J, Loeuille D, Weber U, Zubler V, Roemer FW, Jaremko JL, Sayre EC & Lambert RG (2014). Preliminary validation of 2 magnetic resonance image scoring systems for osteoarthritis of the hip according to the OMERACT filter. *J Rheumatol* **41**, 370-8.

34. Javaid MK, Kiran A, Guermazi A, Kwoh CK, Zaim S, Carbone L, Harris T, McCulloch CE, Arden NK, Lane NE, Felson D & Nevitt M (2012). Individual magnetic resonance imaging and radiographic features of knee osteoarthritis in subjects with unilateral knee pain: the health, aging, and body composition study. *Arthritis Rheum* **64**, 3246-55.

35. Potter HG & Schachar J (2010). High resolution noncontrast MRI of the hip. *J Magn Reson Imaging* **31**, 268-78.

36. Palle J, Wittig NK, Østergaard M, Jensen AB, Birkedal H, Müller B & Wang G, *The osteocyte lacuno-canalicular network in bone investigated by synchrotron radiation-based techniques*, in *Developments in X-Ray Tomography XII*. 2019.

37. Dong P, Haupert S, Hesse B, Langer M, Gouttenoire PJ, Bousson V & Peyrin F (2014). 3D osteocyte lacunar morphometric properties and distributions in human femoral cortical bone using synchrotron radiation micro-CT images. *Bone* **60**, 172-85.

38. Tiede-Lewis LM & Dallas SL (2019). Changes in the osteocyte lacunocanalicular network with aging. *Bone* **122**, 101-113.

39. Walsh DA, McWilliams DF, Turley MJ, Dixon MR, Fransès RE, Mapp PI & Wilson D (2010). Angiogenesis and nerve growth factor at the osteochondral junction in rheumatoid arthritis and osteoarthritis. *Rheumatology (Oxford)* **49**, 1852-61.

40. Muratovic D, Findlay DM, Cicuttini FM, Wluka AE, Lee YR & Kuliwaba JS (2018). Bone matrix microdamage and vascular changes characterize bone marrow lesions in the subchondral bone of knee osteoarthritis. *Bone* **108**, 193-201.

41. Muratovic D, Findlay DM, Cicuttini FM, Wluka AE, Lee YR, Edwards S & Kuliwaba JS (2019). Bone marrow lesions in knee osteoarthritis: regional differences in tibial subchondral bone microstructure and their association with cartilage degeneration. *Osteoarthritis Cartilage*

42. Wluka AE, Hanna F, Davies-Tuck M, Wang Y, Bell RJ, Davis SR, Adams J & Cicuttini FM (2009). Bone marrow lesions predict increase in knee cartilage defects and loss of cartilage volume in middle-aged women without knee pain over 2 years. *Annals of the Rheumatic Diseases* **68**, 850-855.

43. Muratovic D, Cicuttini F, Wluka A, Findlay D, Wang Y, Otto S, Taylor D, Humphries J, Lee Y, Labrinidis A, Williams R & Kuliwaba J (2016). Bone marrow lesions detected by specific combination of MRI sequences are associated with severity of osteochondral degeneration. *Arthritis Res Ther* **18**, 54.

44. Hintermüller C, Marone, F., Isenegger, A., Stampanoni, M (2010). Image processing pipeline for synchrotron-radiation-based tomographic microscopy. Journal of Synchrotron Radiation **17**, 550-559.

45. Paganin D, Mayo SC, Gureyev TE, Miller PR & Wilkins SW (2002). Simultaneous phase and amplitude extraction from a single defocused image of a homogeneous object. *J Microsc* **206**, 33-40.

46. Marone F, Stampanoni, M (2012,). Regridding reconstruction algorithm for real-time tomographic imaging. *Journal of Synchrotron Radiation* **19**, 1029-1037.

47. Hemmatian H, Laurent MR, Ghazanfari S, Vanderschueren D, Bakker AD, Klein-Nulend J & van Lenthe GH (2017). Accuracy and reproducibility of mouse cortical bone microporosity as quantified by desktop microcomputed tomography. *PLoS One* **12**, e0182996.

48. Fazzalari NL & Parkinson IH (1997). Fractal properties of subchondral cancellous bone in severe osteoarthritis of the hip. *J Bone Miner Res* **12**, 632-40.

49. Chappard C, Peyrin F, Bonnassie A, Lemineur G, Brunet-Imbault B, Lespessailles E & Benhamou CL (2006). Subchondral bone micro-architectural alterations in osteoarthritis: A synchrotron micro-computed tomography study. *Osteoarthritis and Cartilage* **14**, 215-223.

50. Zaino CJ, Leali A & Fetto JF (2010). Regional variations of bone quantity and quality impact femoral head collapse. *Clin Orthop Relat Res* **468**, 276-82.

51. Grynpas MD, Alpert B, Katz I, Lieberman I & Pritzker KP (1991). Subchondral bone in osteoarthritis. *Calcif Tissue Int* **49**, 20-6.

52. Finnila MAJ, Thevenot J, Aho OM, Tiitu V, Rautiainen J, Kauppinen S, Nieminen MT, Pritzker K, Valkealahti M, Lehenkari P & Saarakkala S (2017). Association between subchondral bone structure and osteoarthritis histopathological grade. *J Orthop Res* **35**, 785-792.

53. Li B, Marshall D, Roe M & Aspden RM (1999). The electron microscope appearance of the subchondral bone plate in the human femoral head in osteoarthritis and osteoporosis. *J Anat* **195 (Pt 1)**, 101-10.

54. Fazzalari NL & Parkinson IH (1998). Femoral trabecular bone of osteoarthritic and normal subjects in an age and sex matched group. *Osteoarthritis Cartilage* **6**, 377-82.

55. Intema F, Hazewinkel HA, Gouwens D, Bijlsma JW, Weinans H, Lafeber FP & Mastbergen SC (2010). In early OA, thinning of the subchondral plate is directly related to cartilage damage: results from a canine ACLT-meniscectomy model. *Osteoarthritis Cartilage* **18**, 691-8.

56. Shimamura M, Iwata K, Mashiba T & Yamamoto T (2017). Accumulation of microdamage in subchondral bone at the femoral head in patients with osteoarthritis of the hip. *Journal of Orthopaedic Research* **35**,

57. Cui WQ, Won YY, Baek MH, Lee DH, Chung YS, Hur JH & Ma YZ (2008). Age-and region-dependent changes in three-dimensional microstructural properties of proximal femoral trabeculae. *Osteoporos Int* **19**, 1579-87.

58. Chiba K, Burghardt AJ, Osaki M & Majumdar S (2013). Heterogeneity of bone microstructure in the femoral head in patients with osteoporosis: an ex vivo HR-pQCT study. *Bone* **56**, 139-46.

59. Chiba K, Burghardt AJ, Osaki M & Majumdar S (2014). Three-dimensional analysis of subchondral cysts in hip osteoarthritis: an ex vivo HR-pQCT study. *Bone* **66**, 140-5.

60. Lv H, Zhang L, Yang F, Li M, Yin P, Su X, Yin P, Zhang L & Tang P (2015). A novel 3D-printed device for localization and extraction of trabeculae from human femoral heads: a comparison with traditional visual extraction. *Osteoporosis International* **26**, 1791-1799.

61. Tanamas SK, Wluka AE, Pelletier JP, Pelletier JM, Abram F, Berry PA, Wang Y, Jones G & Cicuttini FM (2010). Bone marrow lesions in people with knee osteoarthritis predict progression of disease and joint replacement: A longitudinal study. *Rheumatology* **49**, 2413-2419.

62. Turmezei TD, Lomas DJ, Hopper MA & Poole KES (2014). Severity mapping of the proximal femur: A new method for assessing hip osteoarthritis with computed tomography. *Osteoarthritis and Cartilage* **22**, 1488-1498.

63. Li G, Zheng Q, Landao-Bassonga E, Cheng TS, Pavlos NJ, Ma Y, Zhang C & Zheng MH (2015). Influence of age and gender on microarchitecture and bone remodeling in subchondral bone of the osteoarthritic femoral head. *Bone* **77**, 91-7.

64. Neumann G, Mendicuti AD, Zou KH, Minas T, Coblyn J, Winalski CS & Lang P (2007). Prevalence of labral tears and cartilage loss in patients with mechanical symptoms of the hip: evaluation using MR arthrography. *Osteoarthritis Cartilage* **15**, 909-17.

65. Jaremko JL, Lambert RG, Zubler V, Weber U, Loeuille D, Roemer FW, Cibere J, Pianta M, Gracey D, Conaghan P, Ostergaard M & Maksymowych WP (2014). Methodologies for semiquantitative evaluation of hip osteoarthritis by magnetic resonance imaging: approaches based on the whole organ and focused on active lesions. *J Rheumatol* **41**, 359-69.

66. Kim C, Nevitt MC, Niu J, Clancy MM, Lane NE, Link TM, Vlad S, Tolstykh I, Jungmann PM, Felson DT & Guermazi A (2015). Association of hip pain with radiographic evidence of hip osteoarthritis: diagnostic test study. *Bmj* **351**, h5983.

67. Suri S & Walsh DA (2012). Osteochondral alterations in osteoarthritis. *Bone* **51**, 204-211.

68. Kerschnitzki M, Kollmannsberger P, Burghammer M, Duda GN, Weinkamer R, Wagermaier W & Fratzl P (2013). Architecture of the osteocyte network correlates with bone material quality. *J Bone Miner Res* **28**, 1837-45.

69. Vashishth D, Koontz J, Qiu SJ, Lundin-Cannon D, Yeni YN, Schaffler MB & Fyhrie DP (2000). In vivo diffuse damage in human vertebral trabecular bone. *Bone* **26**, 147-52.

70. Vatsa A, Breuls RG, Semeins CM, Salmon PL, Smit TH & Klein-Nulend J (2008). Osteocyte morphology in fibula and calvaria --- is there a role for mechanosensing? *Bone* **43**, 452-8.

71. van Hove RP, Nolte PA, Vatsa A, Semeins CM, Salmon PL, Smit TH & Klein-Nulend J (2009). Osteocyte morphology in human tibiae of different bone pathologies with different bone mineral density--is there a role for mechanosensing? *Bone* **45**, 321-9.

72. Carter Y, Thomas CD, Clement JG, Peele AG, Hannah K & Cooper DM (2013). Variation in osteocyte lacunar morphology and density in the human femur--a synchrotron radiation micro-CT study. *Bone* **52**, 126-32.

73. Mader KS, Schneider P, Müller R & Stampanoni M (2013). A quantitative framework for the 3D characterization of the osteocyte lacunar system. *Bone* **57**, 142-54.